DEPARMENT OF METEOROLOGY

THE UNIVERSITY OF READING

Investigation of climate effects on the global atmospheric electrical circuit using surface potential gradient data

SIMON A. KING

A dissertation submitted in partial fulfilment of the requirement for the degree of Master of Science in Applied Meteorology

August 2004

Abstract

Global temperature changes have been suggested as a source of variability in the global atmospheric electrical circuit, but little data has been available for investigation. New data of potential gradient (PG) has been discovered from Kew Observatory, London and provides the longest time series of atmospheric electricity for investigation into a link between the global electrical circuit and temperature changes.

Changes in the global atmospheric electric circuit are important with regard to modern climate change issues as a possible increase in lightning frequency can indirectly regulate tropospheric ozone and CO_2. These greenhouse gases are important constituents of the enhanced greenhouse effect and lead to increases in global temperature, creating a positive feedback

In the UK, atmospheric PG measurements have been made at Kew since the installation of the Kelvin water-dropper electrometer in 1843. Continuous measurements of PG at Kew exist from 1877-1979 giving the longest known record of the atmospheric electrical circuit in the world. However, measurements made from 1877-1898 have never been calibrated or analysed.

PG measurements made at Kew have been influenced by local smoke pollution, which masks the global electrical signal. After investigation into the annual and diurnal cycle of the PG, the time when measurements are less influenced by smoke pollution is during the summer months at approximately 1430 UT.

In this dissertation, an absolute calibration of PG between 1877 and 1898 at 1430 UT in June from Kew was successfully achieved using a measure of the geomagnetic *aa*-index. Using the newly calibrated PG data from Kew with existing calibrated measurements from 1877-1931, a decreasing trend in atmospheric PG at Kew of 0.32% per year is evident.

Measurements of atmospheric electricity have been shown to link with near surface air temperatures both globally and in the tropics. This hypothesis has been investigated using the PG data from 1877 to 1931. It was found that; (i) the response of the global atmospheric PG with tropical near surface temperatures is a 37% change in PG per 1^oC change in temperature and (ii) there is a 25% change in PG with a 1^oC change in global near surface air temperatures.

Contents

Chapter 1 - Introduction

Lightning and atmospheric electricity have been studied for many years, but the existence of an electrical atmosphere on Earth was around even before life evolved on Earth about three billion years ago. It has even been suggested by some (Miller, 1953) that lightning played a role in producing the organic molecules necessary for the formation of every life form. Fossil evidence is also available of lightning strikes from 250 million years ago, called fulgurite. The first encounter of human life and lightning may have been both frightening and fascinating and these civilizations incorporated lightning and thunder with religious beliefs.

Serious studies of lightning and the electrical atmosphere were conducted by Benjamin Franklin, Thomas Francois D'Alibard and John Canton more than 200 years ago (Chalmers, 1967). With the invention of the Leyden Jar – the first electrical condenser consisting of a glass bottle lined inside and outside with tin foil in which a charge could be stored for some time (Chalmers, 1967) – investigations began into electric discharges. Frankin (1750) wanted to collect electricity from thunder clouds by means of a point on a high tower, though D'Alibard (1752) was the first to conduct this experiment by using an iron rod 40ft high. This experiment was successful on 10 May 1752 when sparks from the earthed rod were noticed. A month later, Chalmers (1967) describes how Franklin obtained the same results with his famous kite and key experiment. John Canton was the first English scientist to verify the theory by Franklin and D'Alibard during a storm in London on 20 July 1752. Canton used a three foot tin rod attached to an 18 inch insulating glass rod that had needles attached to the rod. During the storm he felt and saw an electric spark pass between his knuckle and the rod. These experiments lead to the first lightning rod which was used in the study of lightning and then later as a safety mechanism by directing a lightning bolt to Earth to prevent the damage of high buildings such as churches (Uman and Rakov, 2003, Chalmers, 1967).

In more recent times, one of the most influential scientists in atmospheric electricity was a Scottish Professor, Sir William Thomson (Later lord Kelvin). Lord Kelvin recognized the electrical state of the atmosphere as a vertical electric field and introduced the concept of potential (Israel, 1970). Kelvin also produced the first true precision instrument for measuring potential in the atmosphere – the water-dropper electrometer. Everett (1863) describes the instrument as an insulated copper can having a brass pipe leading from it, through which a fine stream of water can be discharged by turning a tap. The electrometer measures a charge that is created when the stream of fine water breaks into drops in the atmosphere.

Lord Kelvin's instrument – the Thomson water-dropper combined with a quadrant electrometer was in use at Kew Observatory, near London (51°28'N, 0°19'W) since its instillation in the early 1860's (Everett, 1868). In its early times the instrument was only used periodically as numerous scientist carried out experiments. Though, since 1876, Thomson's electrometer and other improved instruments have been in use to provide a continuous record of potential at Kew Observatory (until its closure in 1981) and other sites such as the Eiffel Tower in Paris, France (Harrison and Aplin, 2003).

In the latest studies regarding the electrical nature of the atmosphere, climate change has been recognized as possible feature, as influenced by its importance in atmospheric science. More specifically, investigations have led scientists to correlate changes in atmospheric electricity with temperature changes across the globe. Williams (1992, 1994) has been in the forefront of these investigations with suggestions that as tropical near surface air temperatures increase by 1°C, lightning frequency will increase by 10%. Variations of this hypothesis have resulted in similar conclusions using data limited to geographical areas. Other studies have looked at the change in the global distribution of lightning, the changes in tropospheric chemistry and the role of aerosols in the atmosphere. These aspects are all linked to changes in the electrical circuit and a changing climate.

In this dissertation, the hypothesis of a temperature sensitivity of the global electrical circuit presented by Williams (1992, 1994) is investigated using a long time series of atmospheric electricity data. The main focus of the study is the PG measurements made at Kew Observatory in the period 1877-1898. As yet, this continuous record has not been studied in detail and may prove useful in extending the PG back from the existing 1898-1979 record. These early measurements were made with Thomson's water-dropper electrometer which, at the time was not able to apply an absolute scale value to the measurements. As part of this dissertation, a calibration technique is discussed to permit the early relative values to be compared with absolute measurements post 1898.

Once the calibration is complete, a PG record of 102 years (1877-1979) is available for additional investigation. Further investigation into the PG measurements includes an analysis in the trend of PG throughout a 56 year period. This is coupled with global and tropical temperature records in the same period where a sensitivity of a change in PG with temperature can be obtained.

Literature in this study includes an explanation of the global atmospheric circuit presented in section two. This chapter introduces the global electrical circuit with brief introduction to aspects of the physics behind the circuit. Chapter three presents a climate change aspect to the electrical

circuit by discussing current results on changes to the circuit with global warming. The feedbacks associated with a changing electric circuit are also discussed with reference to tropospheric chemistry, spatial distribution of components of the circuit and human consequences.

In chapter four, an introduction to the data analysis is made including a history of previous measurements made at Kew Observatory. Chapter five includes preliminary data analysis and illustrates the methods used to obtain a suitable calibration for the 1877-1898 PG measurements. The resulting calibration technique is used and results presented in chapter six

The primary findings from the calibration and analysis of new PG data shows a strong relationship between tropical near surface air temperatures and PG, with a sensitivity of 39% per unit degree change in temperature. However, investigation into global temperature variations and PG shows a 24% per unit degree change in temperature, where the correlation was not as strong as the tropical temperature relationship. These results and further discussions are presented in more detail with the conclusions in chapter seven.

Chapter 2 - The global atmospheric electric circuit

2.1 Introduction

During fair weather days there is an electrical current that travels vertically downwards from the upper atmosphere towards the Earth's surface. The electric field measured at the Earths surface is approximately 100-300 volts per meter (V/m) but this is not apparent in everyday life, as virtually everything around us is a good conductor compared to air (i.e. materials that contain a large number of electrons that are free to move). This means that we do not encounter a 1 kV potential difference when getting into a car on an upper floor in a parking garage, as described by Bering *et al.,* (1999). Atmospheric electricity was established in the early 1700's when Benjamin Frankin proposed a concept that lightning was an electrical phenomenon in the atmosphere. Franklin went further to prove this by conducting many experiments including the famous kite experiment where electricity was conducted through the string of the kite. Many other scientists worked on lightning and electricity but it wasn't until 1752 when Lemonnier (1752) and John Canton (Chalmers, 1967) first found effects of electricity in fine weather. His experiment used a wooden pole with a pointed iron rod fixed to the top with an iron wire that entered a building without making any contact, ending on stretched silk fibre. In addition to finding sparks under disturbed thunder conditions, Lemonnier found that particles of dust were also attracted to the iron wire when electrified under fair weather conditions. This method showed that electricity was present in the atmosphere that is not strong enough to produce lightning sparks (Chalmers, 1967).

2.2 Structure of the global atmospheric electrical circuit

The global circuit consists of the ionosphere, Earth's surface, fair-weather current and thunderstorm current. The ionosphere is approximately 80 Km in the upper atmosphere and is considered as a conductive plate that is positively charged with a potential (the Ionospheric potential, V_I) of about 250-300 kV (Alderman and Williams, 1996; Bering *et al.,* 1998). The Earth's surface is negatively charged and is part of the inner shell that can be compared loosely with a spherical capacitor, with the ionosphere making up the outer equipotential shell. Figure 2.1 shows a summary of the global circuit.

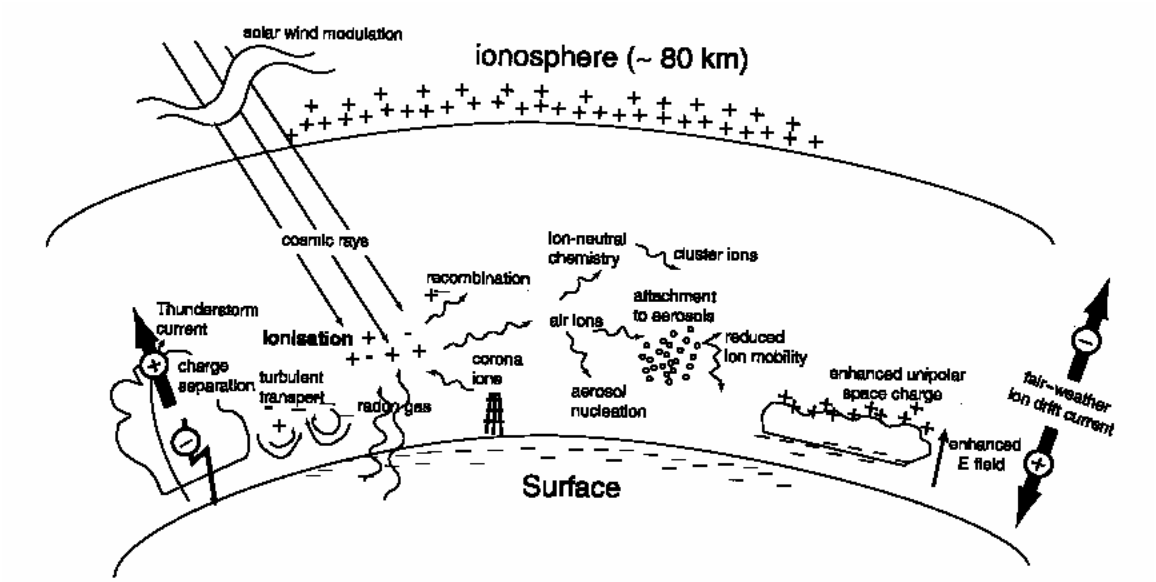

Figure 2.1. Illustrating of the global electrical circuit. Four main components of circuit are the positively charged Ionosphere, negatively charged surface, the fair-weather current and thunderstorm activity bringing negative charge to the surface and positive charge to Ionosphere, closing the circuit. (Taken from Harrison and Carslaw, 2003)

Within the ionosphere, the positive charge is carried to areas of fair weather, and small currents flows vertically – the fair-weather current. In order for the spherical capacitor to remain charged, there must be a mechanism that acts to re-supply the charge to close the electrical circuit. Wilson (1920) suggested that the negative charge of the Earth's surface is maintained by disturbed weather activity. Thunderstorms are the most common forms of disturbed weather that cause local electric fields to be produced and cause positive charge to move upwards toward the ionosphere and negative charge to move to the surface – known as charge separation.

The ionospheric potential and the Earth-air current form part of the Direct Current (DC) circuit, which is discussed in section 2.4. There is also an Alternating Current (AC) circuit within the global circuit, which causes the neutral atmosphere to behave like a resonant cavity waveguide when excited by ultra-low frequency electromagnetic radiation, causing resonances at a range of frequencies. This is described in detail in the next section.

2.3 AC circuit

The resonances caused by the ultra-low frequency electromagnetic radiation, as mentioned above, range in a spectrum of frequencies at 7.8-45 Hz and are called the Schumann Resonances (SR) (Rakov and Uman 2003). These resonances are excited by electromagnetic emissions from lightning strokes and can be regarded as excitations of the AC global circuit (Bering *et al.*, 1999).

The amplitude of the SR at any given time and location can be determined by the integrated effect of the worldwide lightning activity at that time. It has been reported by Price (1993) that there are approximately 2000 thunderstorms active at any one time around the globe that are continuously charging the atmospheric capacitor. Because the SR is excited from lightning strokes, there have been suggestions that local measurements of the resonance determine lightning activity in tropical thunderstorms (Sentman and Fraser, 1991). Williams (1992) highlighted one problem with this theory, which is that changes in cavity shape caused by changes in ionization in the upper atmosphere can increase or decrease the electromagnetic frequency provided by a lightning strike. This is linked with the diurnal changes in the global electric circuit, discussed in further detail later.

An important issue with moving on from the SR connection with tropical thunderstorm activity is discussed by Williams (1992) who suggests that by measuring the SR we might be able to deduce tropical temperature changes. Theory suggests that lightning activity is controlled by cloud electrification and the interaction of ice particles in the upper troposphere (Williams, 1992). Williams (1992) continues to suggest that buoyancy is non-linearly related to cloud electrification processes and buoyancy in turn is controlled by surface air temperatures. Tropical thunderstorm activity is of interest here because lightning activity increases with the depth and vigour of convection and we know that convection is deeper and more frequent in the tropics.

Observations of lightning from satellite show that approximately two of every three lightning flashes occur in the latitude interval $\pm 23^{o}$ (see figure 2.2) and that tropical land areas have a higher frequency of lightning than do the central oceans (Williams, 1992). There have been a number of studies that have compared wet-bulb temperatures with lightning flash counts in order to infer an association between lightning and temperature.

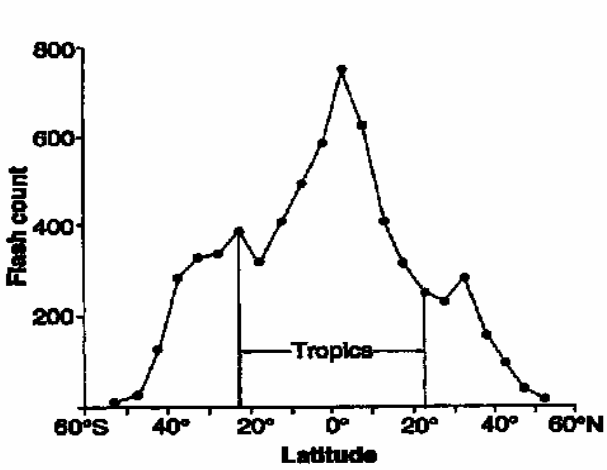

Figure 2.2. Diagram of the distribution of lightning counts across the latitude band ±60^{o} showing peak lightning activity in the tropics from Williams (1992).

Mackerras (1985) used data from Darwin, Australia, and showed that monthly mean lightning counts increased more than two orders of magnitude as the wet-bulb temperature increased from 25^{o}C to 27^{o}C. Similar studies have been made at locations such as Kourou, French Guiana and South America (Williams, 1992) which show a similar sensitivity in temperature changes with a 2^{o}C change in wet-bulb temperature corresponding with a 20-fold increase in lightning activity.

Williams (1992) examined a time series of SR magnetic field data from Kingston, Rhode Island, to further test the idea that SR could behave as a sensitive global tropical thermometer on a timescale of months to years. Results from this study showed the SR amplitude following the dry-bulb temperature record very closely with warmer periods showing an enhanced SR magnitude and cooler periods with suppressed amplitude.

Price (2000), highlighted that the SR can be measured at a single station around the globe, which can be used to represent the SR for the whole globe. At extremely low frequencies, the radiation produced by a lightning flash can propagate a few times around the world before dissipating, as they are trapped in the ionosphere-surface waveguide. Results from simultaneous measurements of the SR in Israel and California showed that there is a correlation of 0.9 between the two stations over a 25 year period in 1998. Therefore, Price (2000) suggests that a single station can be used to track global lightning variability.

2.4 DC circuit

2.4.1 Fair weather current

The fair-weather current, as briefly mentioned in section 2.1, is the flow of current from the positively charged ionosphere to the negatively charged Earth's surface in regions of fair-weather. A fair-weather condition is one where no local processes of charge separation that contributes any additional electric field (i.e. regions where no thunderstorm activity takes place) and where the electric field is steady, modulated only by the global circuit (Harrison, 2003). A voltage gradient can be measured that is caused by a large potential difference between the lowest layer of the ionosphere and surface. This is a positive current (downward current) that has been estimated between 100-150 V/m (Rakov and Uman, 2003; Harrison, 2002).

Measurement of the fair-weather current can be made through a variety of methods such as Kelvin's water dropper electrometer, quadrant electrometer (Scrase, 1934) and the universal portable electrometer (Wilson, 1916). One set of continuous measurement of the current were made using Kelvin's water dropper electrometer at Kew Observatory, made from 1876 to the 1930's. In theory the fair-weather current is part of the global electrical circuit and should be measurable anywhere in the globe and give representative results for the globe. In reality this is not completely possible, as there are local effects that can amplify or distort the electrical signal. Records obtained from continental stations around the globe have all been studied and variations in cloud cover, humidity, total aerosols (discussed in section 2.5) and topography around the station can modify or dominate the global electric field (Krider and Roble, 1986). One solution to this problem is to make measurements in a totally clean environment, where no local effects can interfere with the electric field. Data over open ocean waters is such a place and measurements were made during 1915-1929 by the research vessel Carnegie.

The Carnegie research showed a strong diurnal, seasonal and annual variation in the fair-weather electric field. This original data is now seen as an important discovery in the variation of the global electrical circuit and many other studies have resulted from this. Figure 2.3 below shows the diurnal variation of the PG as measured during the Carnegie research. The diurnal variation in the global electric field shows a maximum at 1830 UT (Universal Time) and a minimum at 0230 UT.

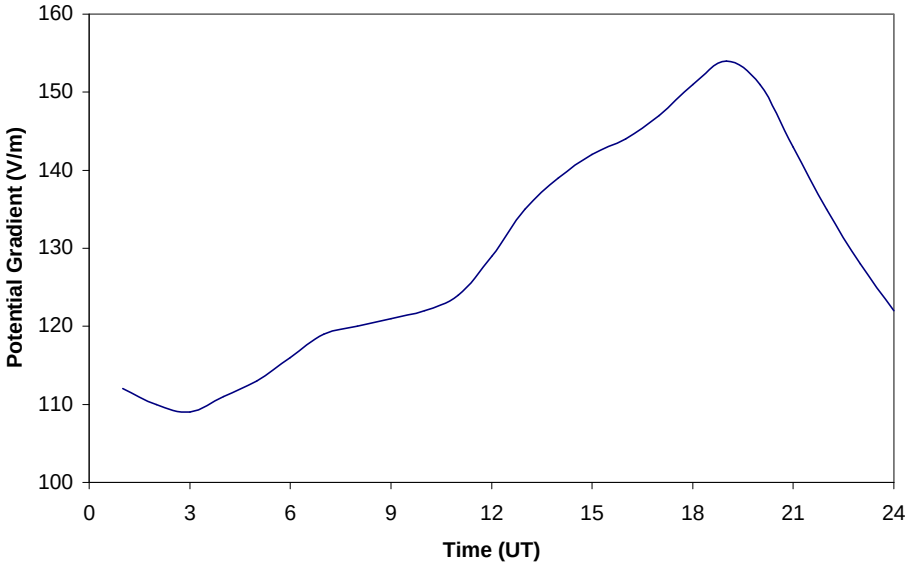

Figure 2.3. The average diurnal variation of PG as measured by the Carnegie research vessel during 1915-1919. (Adapted from Price, 1993)

In order to establish an annual or inter-annual variation in the electric circuit, the Carnegie data is averaged to remove the diurnal variation. A maximum in electric field in the northern hemisphere winter was found (Parkinson and Torreson, 1931). However, later analysis of the original data by Alderman and Williams (1996) shows the maximum in PG actually occurs in the northern hemisphere summer and not the winter as originally thought. Another study by Hogg (1950) showed the average electric current for 17 continental stations to have a semi-annual variation, with maxima in February and October. Cobb (1968) pointed out that there were a number of errors with Hogg's (1950) work and could not be taken as the truth.

2.4.2 Ionospheric potential

The ionospheric potential, V_I, is a measure of the potential difference between the ionosphere and the Earth's surface. This method of measuring the DC circuit has been used in a couple of studies. It has been suggested by many (Markson *et al.*, 1999; Price 1993) that the ionospheric potential can be used as a proxy index for monitoring variations in global temperature and that only a single sounding is required to achieve a globally representative value. This is essentially because the ionosphere can be considered as an equipotential at latitudes below the polar cap region at any sub-auroral location with fair-weather conditions (Markson *et al.*, 1999). This theory was tested by monitoring the V_I at two locations across the globe simultaneously; Weston, MA and Darwin, Australia. The results showed the Darwin data corresponding with the established Carnegie diurnal variation within 10%, whereas the Weston data was more variable and too large. The

discrepancy in the two datasets is most certainly due to the presence of pollution in Weston while measurements were carried out.

Using ionospheric potential as a proxy for global temperature variations has been suggested because temperature essentially controls convective activity and therefore thunderstorms and electrified shower clouds (the generators maintaining V_I). Markson and Lane-Smith (1994) used radiosonde balloons and 31 electric field soundings of V_I were gathered in August and September 1992. Results suggested a relationship between global temperature from the low latitudes and the V_I measurements. They also found the relationship more evident in the American continent. The authors conclude this was due to the measurements taken in the afternoon when temperature-forced convection was activated and thunderstorms were the major contributor to the global generator.

Markson and Price (1999) used three different methods of ascertaining global surface temperature; i) International Cloud Climatological Project (ISCCP) satellite data, ii) TIROS Operational Vertical Sounder (TOVS) satellite data and iii) National Meteorological Centre surface data. In each case measurements of the ionospheric potential were compared and the authors suggest a 1% increase in temperature corresponds to about a 15% increase in V_I. In another study by Price (1993), a 1% change in global temperature would cause a 20% change in V_I.

As with the air-Earth current, there is also evidence of a diurnal variation in the ionospheric potential. Measurements of ionospheric potential were made for one day at a number of locations across the globe and all compare well with the diurnal cycle of the Carnegie curve at all locations (Muhleisen, 1971; Markson, 1985). This further supports the idea that a single point measurement of V_I gives a globally representative parameter of the global circuit. However, caution should be made as the measurements were made on one particular day only and therefore, major sampling errors giving unreliable results could exist.

2.5 Aerosols

As mentioned in the previous, aerosols in the local atmosphere can mask the global electrical circuit. This is a common problem in many measurements of the DC current and has only recently been quantified as an error in previous studies. Ion-aerosol theory is discussed in section 2.5.1 followed by some evidence of aerosol interaction with the atmospheric electrical circuit in section 2.5.2.

2.5.1 Ion-aerosol theory

Ion-aerosol theory explained here has been summarised from work carried out by Harrison and Aplin (2002). Ions in the atmosphere travel vertically between the ionosphere and earth in a current known as the air-earth current. In air of varying conductivity (σ), the PG and air-earth current (J) can be explained by Ohm's law shown in equation 2.1 below (Harrison and Aplin, 2002).

$$PG = \frac{J}{\sigma} \tag{2.1}$$

Where the conductivity can be explained by equation 2.2 when negative and positive ion concentrations are considered equal.

$$\sigma = 2n\mu e \tag{2.2}$$

where; n is the ion number concentration,
μ is the mean ion mobility, and
e is the electronic charge.

Ion concentrations in the atmosphere are essentially governed by the rate of ion production and removal rates. Harrison and Aplin (2002) suggest that ions are produced by radioactivity and cosmic ray ionization with the removal of ions caused by self-recombination and attachment to aerosol particles in the atmosphere. The production and removal of ions in the atmosphere is assumed balanced and the time variation in the ion number concentration can be represented as shown in equation 2.3 (Harrison and Carslaw, 2003).

$$\frac{dn}{dt} = q - \alpha n^2 - \beta nZ \tag{2.3}$$

where; q is the volumetric ion formation rate,
n is the ion number concentration,
α is the ion recombination coefficient,
β is the ion-aerosol attachment coefficient, and
Z is the monodisperse (all aerosols have same radius) aerosol number concentration.

The first two terms on the right hand side of equation 2.3 represent the balance of ion production and removal in a clean, aerosol-free atmosphere and the last term on the right hand side represents the removal of ions by interaction with aerosol. In a steady state situation with a clean air atmosphere, the removal of ions via aerosol interaction is negligible and βnZ becomes zero. Therefore, equation 2.3 becomes (Harrison and Aplin, 2002);

$$n = \sqrt{\frac{q}{\alpha}} \qquad \textbf{(2.4)}$$

This relationship is substituted into equations 2.2 and 2.1 to give the PG as;

$$PG = \frac{\sqrt{\alpha}}{2\mu e}\frac{J}{\sqrt{q}} \qquad \textbf{(2.5)}$$

Using this expression for PG, the air-earth current (J) and ion production rate (q) provide the only variables and so control the PG.

In a polluted atmosphere such as that at Kew Observatory, ion-aerosol attachment dominates over ion recombination i.e. $\beta nZ \gg \alpha n^2$ as the mechanism of ion removal and the steady state ion concentration becomes (Harrison and Aplin, 2002);

$$n = \frac{q}{\beta Z} \qquad \textbf{(2.6)}$$

As with the clean air scenario, this relationship is used in equations 2.2 and 2.1 to give the PG as;

$$PG = \frac{\beta Z}{2\mu e}\frac{J}{q} \qquad \textbf{(2.7)}$$

In this scenario, the PG is directly proportional to the monodisperse aerosol number concentration (Z), providing the air-earth current (J) and ion production (q) rate remain constant.

Use of ion-aerosol theory can explain how a polluted site such as Kew Observatory may show higher PG values than at clean air sites. The PG measured on the Carnegie research vessel show lower values that are typical of an aerosol-free atmosphere. Research at Eskdalemuir, Scotland shows PG values that are typical of both a clean air site and polluted site. Harrison (2004) reports

that PG data at Eskdalemuir shows the Carnegie global circuit diurnal variation in the winter months, but PG values are greater than would be expected from ion-aerosol theory.

2.5.2 Evidence of ion-aerosol interaction

Aerosol in the atmosphere is very important and is sourced from both natural and anthropogenic processes. The biggest natural primary contributor to natural aerosols is sea-salt and charged windblown dust production. Anthropogenic aerosols are formed from a range of emitted pollutants and it is the finer of these aerosol particles that have a significant effect on the electrical conductivity of air. Smoke, for instance is composed of many particles that are less than 0.1 μm in diameter and falls into a category referred to as Aitken condensation nuclei (Israel, 1970).

If the concentration of Aitken nuclei is large, the concentration of small ions in the air is reduced because the small ions are often captured by the aerosol particles. This leads to a reduction in the conductivity of the air and therefore an increase in the local PG (see figure 2.4 below). There have been some studies to establish the magnitude of the change in PG but it is firstly important to investigate the natural background conductivity. Aitken nuclei have a natural seasonal variation which Bigg *et al.*, (1984) has studied in detail by measuring the concentration at five remote sites in the southern hemisphere. All of the five sites showed a seasonal variation with a minimum ranging from 0-400 /cm^3 in the austral winter (southern hemisphere winter). Similar studies in the northern hemisphere by Flyger *et al.*, (1973) showed similar concentrations (300-600 /cm^3). For comparison, concentrations of Aitken nuclei were measured at land stations that ranged from 10 000 /cm^3 in coastal areas to nearly 150 000 /cm^3 in the centre of a large city (Israel, 1970). The seasonal variation of Aitken nuclei in populated areas of the world follow a trend that is opposite to that of the natural variations. Here, Bigg *et al.*, (1984) reports there is a maximum in the local winter and a minimum in the local summer. This is most likely due to the increased production of fossil fuels in the wintertime when temperatures are low and even atmospheric dispersion characteristics favour suppression of pollutants. If there is any pollution at a site where atmospheric electricity is being monitored then it is highly likely that the low conductivity of the local atmosphere will increase the PG, reducing the likelihood of a global signal.

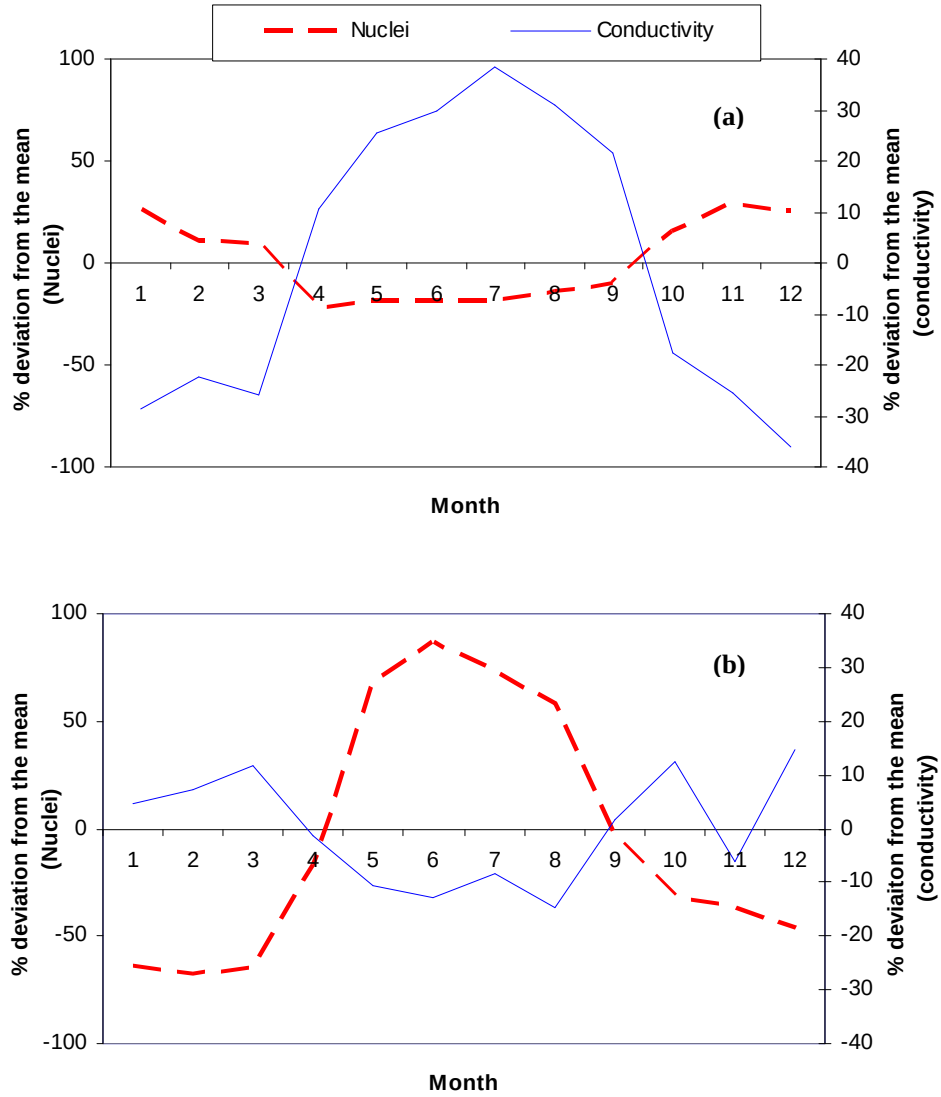

Figure 2.4. (a) Seasonal variation of concentration of Aitken nuclei and electrical conductivity in Poona, India. (b) Seasonal variation of concentration of Aitken nuclei and electrical conductivity in Huancayo, Peru. (Figures adapted from Alderman and Williams, 1996)

Measurements of atmospheric electricity have been used to provide details of pollution occurrences during the nineteenth century in Paris. Because of the effect of aerosol on the PG Harrison and Aplin (2003) used measurements on the Eiffel Tower (285 m) by Chauveau (1925) from 1889 to determine the air pollution levels in the late nineteenth century. Measurements were also made at the surface at the Bureau Central Meteorologique in order to make comparison between a polluted boundary layer and clean air measurements (surface and on top of the Eiffel Tower respectively). Harrison and Aplin's (2003) results show the clean air PG followed the diurnal Carnegie curve. This indicates that measurements made at this level – above the polluted Parisian boundary layer – can be used to measure the global electrical circuit. The diurnal variation of the PG at the surface was found to have a double maximum in summer and autumn,

with a minimum in the middle of the day. The authors of this study suggest the maximum PG at the beginning and end of the day are comparable to the smoke concentration measurements made simultaneously with the PG (Harrison and Aplin, 2003).

The electric field has also been measured at Kew Observatory in the UK from 1843 to 1979 and in a similar study as the Parisian smoke variations; pollution has influenced the PG measurements (Harrison and Aplin, 2002). The study showed the PG diurnal variation to have two maxima at approximately 0900 UT and 2000 UT. This matches the maximum smoke concentrations in the diurnal variation of smoke measurements taken at the same time.

Evidence of clean air electrical measurements comes from a study by Cobb and Phillips (1962) from Mauna Loa Observatory in Hawaii. Mauna Loa Observatory is seen as an ideal location to make continuous measurements of the air-Earth current. The observatory is located at 3.4 km, above the inversion boundary layer for most of the time and is free from local pollution sources. Unpublished measurements taken by Cobb in 1993 (cited in Williams, 1994) in fair weather conditions showed evidence of a diurnal variation similar to the Carnegie curve and an annual signal. The maximum electrical current peak occurred in June and July with the minimum current from December to February. Williams (1994) links these results with the variation of global surface temperature throughout the year.

2.6 Comparison of AC and DC circuits

Both AC and DC circuits have been used to deduce the global electrical circuit and the range of timescale variations from diurnal to annual that correlate with lightning counts, global surface temperature and pollution occurrences. There is possibility that monitoring both the SR and the ionospheric potential can be used to infer a measure of global temperature and global rainfall rates. Bering *et al.*, (1999) suggests that if 60% of the average ionospheric potential arises from electrified rain cloud currents it can possibly be used as a proxy for global rainfall rates.

The SR and ionospheric potential were simultaneously measured in Kingston, Rhode Island and the Bahamas respectively to within ±30 minutes of the recorded UT (Williams, 1992). Each dataset was not considered to have any local weather or pollution effects and the uncertainty in ionospheric potential and SR were calculated as 5 and 10% respectively. The data, shown in figure 2.5, has a strong correlation and supports the theory of a global signal in single station electric circuit measurements.

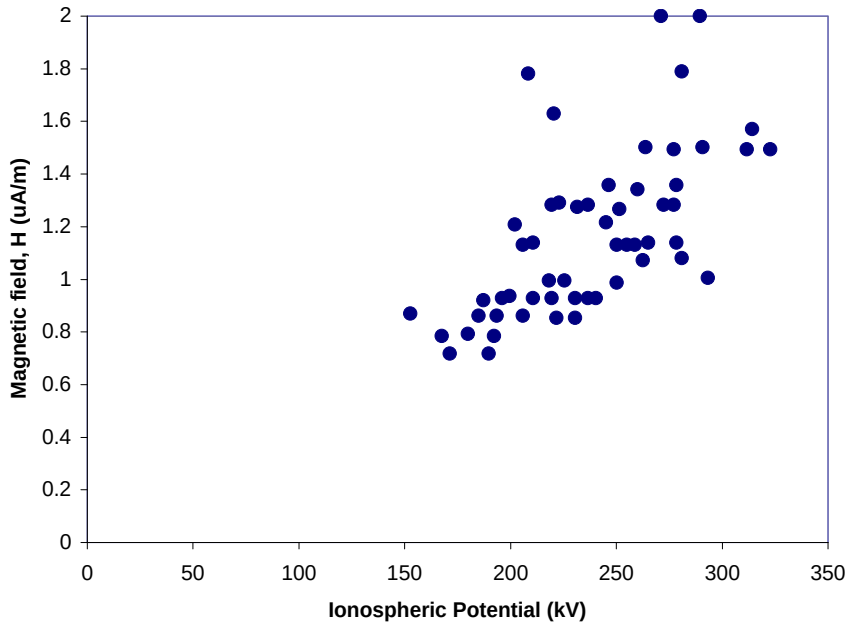

Figure 2.5. Positive correlation of magnetic field data inferred from the SR and ionospheric potential measurements at Kingston, Rhode Island and Bahamas respectively. (Adapted from Williams, 1992)

Chapter 3 - Global atmospheric electric circuit and Climate change

3.1 Introduction

Global temperature records have been reconstructed to the beginning of instrumental records from around 1860, which are central in discussion of climate change. In the United Kingdom, temperature records exist from the Central England Temperature series that began in 1698. Records of atmospheric electricity have been made for over two centuries with early measurements made in 1752 by Lemonnier (see section 2.1). Continuous records of PG started at Kew Observatory, near London in 1876. As the primary motivation of this study, global temperatures and PG measurements are investigated for links. In climate change studies, the importance of investigating the electric circuit and lightning is highlighted in this chapter. Factors such as tropical temperature feedbacks and tropospheric chemistry feedbacks are discussed with some long term implications for society as a result of increasing/decreasing lightning frequency.

3.2 Climate variability and lightning

3.2.1 Temperature variations

Williams (1992) hypothesis was that lightning activity (detected by the SR) provides a proxy for subtle changes in atmospheric temperature changes. Arguing from parcel theory, he reports that lightning is primarily linked with cloud electrification processes and the accumulation of ice particles in the upper troposphere. The cloud electrification processes is controlled by buoyancy within the atmosphere, which in turn is controlled by surface air temperature – the higher the temperature, the more buoyant an air parcel and therefore more vigorous and deep the convection. Williams report focuses on the tropical region where one of the three 'tropical chimneys' is located. Observations in the tropics show that convective available potential energy (CAPE)[1] is determined by the wet-bulb potential temperature at the surface. A 1^{o}C increase in wet-bulb potential temperature in a tropical wet season is equivalent to a CAPE of 1000 J/Kg (Williams, 1992). An increase in CAPE results in an increase in updraft velocity (deduced from equation 3.1) within clouds leading to increased convection, a change in the mass of ice-phase condensate and the gravitational energy available for an ice-based charge separation process.

$$w = 2\sqrt{CAPE} \qquad \textbf{(3.1)}$$

[1] CAPE represents the amount of buoyant energy available to accelerate a parcel vertically. The higher the CAPE value, the more energy available for storm growth (Stull, 2000)

where; w is updraft velocity (ms^{-1}) and,

CAPE is Convective Available Potential Energy ($J\ kg^{-1}$)

Williams (1992) argues that an increase in tropical surface air temperature of $1^{o}C$ will lead to an increase in lightning production of 10%.

3.2.2 Lightning activity

The Optical Transient Detector (OTD) was the first lightning sensor capable of viewing lightning activity both day and night across the globe. (The previous sensor – Defence Meteorological Satellite Program (DMSP) – could only detect lightning in the night time (Makerras and Darveniza, 1998)). By investigating lightning activity by the OTD since its deployment in April 1995, an accurate picture can be made of lightning distribution throughout the globe. Reeve and Toumi (1998) investigated a possible correlation between wet-bulb temperature and OTD data of lightning activity for the globe, the northern hemisphere, southern hemisphere and the tropics. They use large scale averages of the OTD and wet-bulb temperature. The results show the strongest correlation in the northern hemisphere and the weakest in the southern hemisphere. The global correlation was a combination of the two. Contrary to Williams (1992) view that tropical lightning activity has the strongest sensitivity to wet-bulb temperature, Reeve and Toumi (1998) find no significant correlation. They suggest that as Williams (1992) uses tropical local measurements there is possibility for a strong sensitivity on the local scale and not the wider global scale. The difference in the northern and southern hemisphere correlations may be accounted for by the land-ocean ratio. The northern hemisphere has a large land-ocean ratio and therefore is influenced by solar heating leading to deep convection from changes in surface temperatures. In the southern hemisphere, the land-ocean ratio is smaller and the convection is likely to be driven by larger-scale circulation patterns. In a global context however, Reeve and Toumi (1998) predict an average global increase in lightning activity of 40% with a 1 K wet-bulb temperature rise.

In a climate model study, Price and Rind (1994) used the Goddard Institute for Space Studies (GISS) general circulation model to study the possible implications of past and present global lightning frequency. They devised two scenarios; $2xCO_2$ climate (a $4.2^{o}C$ global warming) and a 2% decrease in the solar constant (a $5.9^{o}C$ global cooling). In order to parameterise the lightning frequency, two formulas were used for continental thunderstorms and oceanic thunderstorms, both using convective cloud top height as the predictive value for a lightning occurrence. The continental parameterisation was based on observations showing lightning frequencies related to the fifth power of the cloud height. Results from the model showed that in the warmer climate

scenario ($2xCO_2$), there is a 30% increase in lightning activity and in the colder climate scenario (2% decrease in solar constant) there is a 24% decrease in lightning activity. Price and Rind (1994) conclude that for a 1^oC global warming/cooling there is an approximate 5-6% change in global lightning frequency.

3.3 Tropospheric chemistry and Lightning

3.3.1 Nitrogen and Ozone

The atmosphere is composed of 78% nitrogen, 21% oxygen and 1% of other trace gases such as carbon dioxide, hydrogen and water vapour. Atmospheric electrical discharges such as lightning produce additional trace molecules. Reactive nitrogen species NO_x ($NO+NO_2$) have an important role in influencing tropospheric ozone concentrations. In the troposphere, concentrations of nitrogen oxide, NO and nitrogen dioxide, NO_2 are sufficient to cause an increase in ozone concentration via reaction 3.2 below,

$$NO_2 + h\nu \rightarrow NO + O \qquad \textbf{(3.2)}$$
$$O + O_2 + M \rightarrow O_3 + M$$

In the highest parts of the troposphere / lower stratosphere photochemical processes destroy ozone via reaction 3.3 shown below.

$$NO + O_3 \rightarrow NO_2 + O_2 \qquad \textbf{(3.3)}$$

The major sources of NO_x in the atmosphere are from natural sources such microbial actions in soils, oxidation of atmospheric ammonia, NH_3 and anthropogenic sources such as fossil fuel and biomass burning. The anthropogenic sources are thought to contribute about 77% of tropospheric NO_x (Intergovernmental Panel on Climate Change (IPCC), Third Assessment Report (TAR), 2001). In order to provide global estimates of NO_x production by lightning, an understanding of lightning physical characteristics, chemical mechanisms of NO_x formation by lightning and the global and seasonal lightning distributions is required. These are currently not well characterised (Tie *et al.*, 2002). Estimates of the amount of NO_x produced from a ground lightning flash ranges from $0.23x10^{26}$ to $21x10^{26}$ NO molecules per flash. This leaves uncertainty in the estimation of global NO_x production by lightning (Nesbitt *et al.,* 2000). Estimates range from 9% (Huntrieser *et al.,* 1998) to 23% (Price *et al.,* 1997) of the total global NO_x production, including all anthropogenic and natural sources.

Toumi *et al.*, (1996) modelled the effect of tropospheric ozone from an increase in lightning due to a prescribed global warming using a two-dimensional chemical model. They simulated a 2K warming that caused a doubling in lightning activity. This resulted in an increase in upper tropospheric ozone by 10%, giving a global radiative forcing[2] of +0.3 Wm^{-2}. Sinha and Toumi (1997) suggest this model is somewhat limited as the ability of any model to represent the ozone field accurately is complex and one must assume background NO_x, lightning source strength and the distribution of the NO_x emission with height.

3.3.2 Water vapour

Tropospheric water vapour is an important element in the climate as it is the largest natural greenhouse gas. The impact of water vapour on the climate is still relatively uncertain as it can have a direct effect as a greenhouse gas and an indirect effect through interaction with clouds and aerosols. Price (2000) has suggested that upper-tropospheric water vapour variability and global lightning activity are correlated. He explains the fact that deep continental convective thunderstorms transport large amounts of water vapour into the upper troposphere and thereby dominate the variations of global upper tropospheric water vapour while producing most of the lightning on Earth. Climate models predict a 10% increase in the upper tropospheric water vapour for every 1 K increase in temperature (Price, 2000) while others suggest a 20% rise in water vapour (Rind *et al.*, 1991). It is suggested by Hanson *et al.*, (1984) that while surface temperatures in the tropics may increase by 2-3^{o}C in a warmer climate, the upper tropical troposphere may warm by 6-7^{o}C. A result of this means the upper tropospheric water vapour will increase. An increase in upper tropospheric water vapour will result in less longwave radiation escaping from the atmosphere, leading to amplification in surface temperature. This is a positive feedback

Price (2000) uses the SR as a measure of global lightning activity to compare with upper tropospheric water vapour using NASA Water Vapour Project (NVAP) data. It was found that the sensitivity of this relationship implies for every 0.25 mm increase in equivalent depth of upper troposphere water vapour, the SR signal increases by approximately 25%.

3.3.3 Carbon dioxide

Lightning is a major cause of natural forest fires in mid-latitudes creating an increase in source of CO_2 to the atmosphere. CO_2 is a major greenhouse gas with concentrations in the atmosphere

[2] Radiative forcing – the change in the net vertical irradiance (expressed in watts per square meter) at the troposphere due to an internal change or a change in the external forcing of the climate system. (IPCC, 2001)

increasing from 280 ppm in 1750 to 367 ppm in 1999 (IPCC, 2001). The IPCC (2001) reports that 10-30% of the increase in CO_2 over the past 20 years is predominately due to deforestation (both natural via lightning and anthropogenic via logging). The current radiative forcing of CO_2 in the atmosphere is 1.46 Wm^{-2}. Atmospheric CO_2 is taken up by the ocean because of its high solubility, but the rate of this uptake is limited by the finite speed of vertical mixing through the atmosphere. IPCC (2001) report that the fraction of emitted CO_2 that can be taken up by the oceans and land is expected to decline with increasing CO_2 concentrations. Though lightning-induced CO_2 changes may be small compared with other anthropogenic and natural sources, the importance is highlighted in many studies that an increase in CO_2 ultimately increases the greenhouse effect and contributes to global warming. If this is the case and assuming the suggestion that lightning frequency increases with rises in temperature is correct, a positive feedback is created.

3.4 Lightning hazards in society

A consequence of increased lightning frequency to humans is the hazard of being struck by lightning. In one report, Anderson (2001) reported:

'Lightning struck a supporting steel pole of a tent in which 26 schoolgirls, two adult supervisors, and seven dogs were sleeping. There were injuries to 23 girls, four of which were fatal, and four of the dogs died.'

According to the national meteorological service in the United States (NOAA – National Oceanic and Atmosphere Administration) there are approximately 67 deaths from direct lightning strikes in the US annually. This death toll is the second largest weather related killer in the US after floods. In view of under-reporting of lightning related deaths, the figure is more likely to be 100 people killed a year. Many more people are struck by lightning and survive the strike. Rakov and Uman (2003) report that as many 1000 individuals are injured by lightning a year in the US. Unfortunately, there are no complete records of global estimates of the death toll or injuries, though estimates made by Rakov and Uman (2003) are a few thousand deaths and 5-10 thousand injuries a year.

In terms of injuries caused by lightning; the biggest problems caused are linked with the nervous system which may affect the brain and nervous system. In the long term, a victim often has short term memory loss, seizures, problems multitasking, irritability and personality change. In the short term after the lightning strike, a victim may complain of intense headaches, ringing in the ears, dizziness, nausea and other post-concussion symptoms (NOAA).

As briefly discussed in section 3.3, forest fires are often caused by lightning activity. In the United States, more than 10,000 fires occur every year as a result of lightning at a cost of around $10 million (United States Department of Agriculture (USDA) forest service). The USDA now suggests that forest fires caused by lightning is an important benefit for nature and often many fires started by lightning (away from populated areas) are left to burn. The burning of forests leads to an increase in CO_2 both by the actual biomass burning and by the reduction of forest in up taking CO_2.

Other problems caused by lightning that will not be discussed further here include;

- Property damage – over one billion dollars in insurance claims (Rakov and Uman, 2003).
- Power failures – 30% of all electrical power failures are lightning related (Rakov and Uman, 2003) and,
- Aircraft damage – commercial aircraft are struck by lightning once a year on average (Rakov and Uman, 2003).

The importance of investigating the possible change in the global electrical circuit has been highlighted. It has been shown that for an increase in lightning activity there are a number of climate change feedbacks created by tropospheric chemical reactions. Lightning has also shown to be harmful to both human and ecological life and can cause damage to the world's infrastructure.

Chapter 4 - Introduction to Data analysis

4.1 Introduction

To investigate the hypothesis that changes in the global atmospheric electric circuit is linked with global or tropical temperature changes made in section one; this study is primarily concerned with investigating the suggested links between tropical and global temperature changes with PG measurements made in the UK. In this chapter an introduction is made to the data that will be used in investigating the hypothesis. Firstly, in section 4.2, PG data from the UK is explained in detail then in section 4.3, a discussion is made on the temperature data obtained for the same period.

4.2 PG measurements

4.2.1 History of measurements made at Kew Observatory, London

Atmospheric PG data has been measured in the UK at Kew Observatory, near London semi-continuously which, began by Francis Ronalds (Scrase, 1934) in 1843. Since the beginning of these measurements there have been a few changes at Kew Observatory owing to different methods of observation of the PG. A change in the observation method requires knowledge of how the PG may differ from method to method. Calibration of the PG data is used to compare the different methods, which has been completed for three periods – 1898-1909, 1910-1931 and 1932-1934 (details of these periods is shown in table 4.1), though work is still to be done on some of the earliest measurements (Scrase, 1934). Scrase (1934) describes the earliest measurements from 1843 by Ronalds. They were taken using a lantern collector that was exposed 16 feet above the dome of the observatory, with the electric field being read on Volta's scales on straw electrometers[3]. Measurements taken using this method continued four times a day for two years and then every two hours for the next three years (Scrase, 1934).

The first set of well-characterised measurements was taken using a water dropper electrometer, installed by Lord Kelvin in 1861 (Harrison and Aplin, 2002). The apparatus started as a divided-ring electrometer, using a photographic method of recording. These were not absolute values of PG but were relative values. This was then later replaced by a quadrant electrometer. Scrase (1934) describes that G.M. Whipple was able to determine absolute measures of the deflections of the electrometer needle and express the potential of the collector in terms of volts. It is noteworthy

[3] Two straw pieces suspended from the roof of a lantern collector which diverge at a certain angle once an electric potential is present.

that these measurements were still uncalibrated and so the observations cannot be used for determining whether there has been any change in the mean PG at Kew in the period between 1843 and 1898 (Scrase, 1934). Despite this, many measurements exist and studying these may help in extending the record of PG measurements for a century – the longest known record of the atmospheric electric circuit.

Scrase (1934) describes many experiments and changes in the position of the electrometer at Kew Observatory from 1884 to 1931. He explains that Chree (1896) determined the influence of the observatory building on the water-dropper electrometer. This led to the electrometer being moved to the observatory lawn so that a regular standardisation of absolute PG measurements was made in the open. This method of measurement commenced from 1910 and previous measurements (1898 – 1909) had a correction factor applied to make them comparable to data by the new routine. Measurements made pre 1898 were not corrected as they were only relative values before a scale was introduced from 1898.

An experiment by Watson (1929) in 1926 showed that elevated objects in the observatory neighbourhood affected the measurements made at the lawn site. This led to the building of an underground laboratory under the observatory lawn. Measurements were made on a flat surface away from objects that may cause a disturbance in the PG (Scrase, 1934). The underground laboratory started recording measurements of PG in 1932. Table 4.1 below shows a small summary of data available from Kew Observatory from 1843 to 1979.

Table 4.1. Summary of the different changes in measurements of PG at Kew Observatory from 1843 to 1979.

Time period	Type of Observation
1843 – 1845	Ronalds measured atmospheric electricity four times a day using a collector in the form of a lantern erected 16 feet above the observatory dome. The potential of the collector was read on Volta's scale.
1845 – 1848	Ronalds continued measuring atmospheric electricity using the lantern collector every two hours.
1848 – 1862	No record of any measurements taken in this period
1862 – 1864	Whipple used the non-calibrated Kelvin's water dropper using a divided-ring electrometer giving PG measurements in arbitrary form.
1864 - 1898	Use of non-calibrated Kelvin's water dropper using a quadrant electrometer
1898 – 1909	Electrometer moved to open on the observatory lawn so the observatory building had no influence on the PG measurements.
1910 – 1931	Change in apparatus due to distortion caused by instrument stand.
1932 – 1979	Underground laboratory with measurements taken on flat surface terrain

4.2.2 Current understanding of Kew data

As mentioned previously, PG data from 1877 to 1898 was measured using uncalibrated instruments that gave relative readings of the potential at Kew Observatory. Therefore, this data has not been substantially used in qualitative analysis of the PG at Kew. The majority of the results and conclusions made of the PG have been established using data from 1898 to 1931. This study will be focused mainly on the earliest data set (1877-1898) that is currently archived in the National Archives of the Meteorological Office in Bracknell, UK. To this author's knowledge, the PG data from this period has not been tabulated and is still in its original raw measurement form. This will be explained in more detail in chapter 5. It is also important to comment on the findings of the 1898-1931 data series, as there is no applicable reason why results should vary from the earlier PG measurements.

Scrase (1934) has reported on the PG data from 1898 to 1931 and shows there is a diurnal and annual variation, which shall be discussed in detail.

4.2.2.1 Diurnal variation in PG at Kew

Figure 4.1 below shows monthly averages and diurnal variation from this mean PG for each month in this period. Scrase (1934) notes that there were no appreciable anomalies and only a very limited amount of smoothing was necessary in drawing the curves seen.

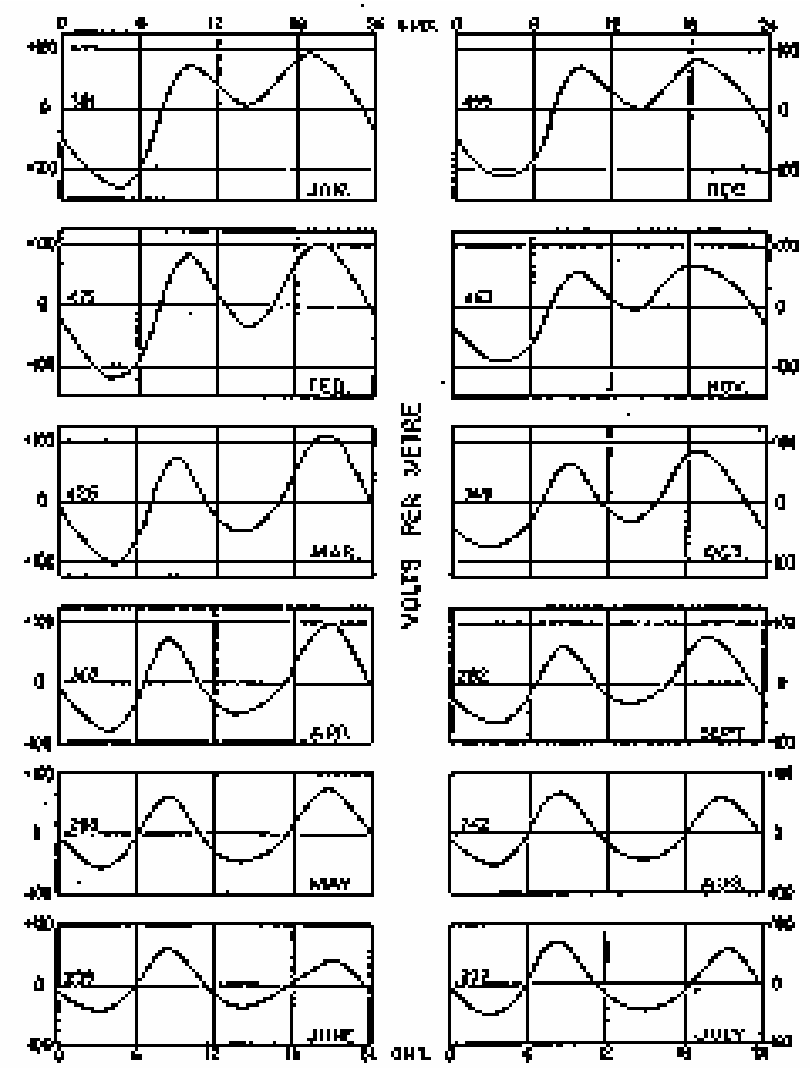

Figure 4.1 Monthly means and the hourly average for that month showing diurnal variation from this mean of PG between 1898 and 1931. Top left plot showing January through to June in the bottom left plot. July can be seen in the bottom right plot through to December in the top right plot. (Taken from Scrase, 1934)

As can be seen from the plots above, there is a well marked double oscillation. The maximum in the evening is greater than the morning maximum except during the summer months (June, July and August) when the evening maximum is larger than the morning maxima. As mentioned in section 2.5, there is evidence that local effects such as pollution can influence the daily variation of PG. Scrase (1934) discusses Whipple's (1929) suggestion that there was a shift in the summer evening maximum due to the introduction of "summer time" (daylight saving hours) in 1916. The author of this report suggests it may have more to do with the reduction in fossil fuel burning during the evening in the summer months, causing a reduction in the local atmospheric smoke concentrations at Kew Observatory. In comparison to the Carnegie diurnal variation, figure 4.2 below shows the average diurnal variation at Kew from 1898 to 1931 with the Carnegie diurnal variation during the periods 1915 to 1921 and 1928 to 1929. It shows the existence of the local

morning maximum at Kew, with no maximum in the Carnegie curve in the morning. Both curves show an evening maximum, though they do not occur at the same time (Scrase, 1934). This is probably due to the later use of fires and smoke production in the summer months when it is warmer and lighter for a longer period in the evening.

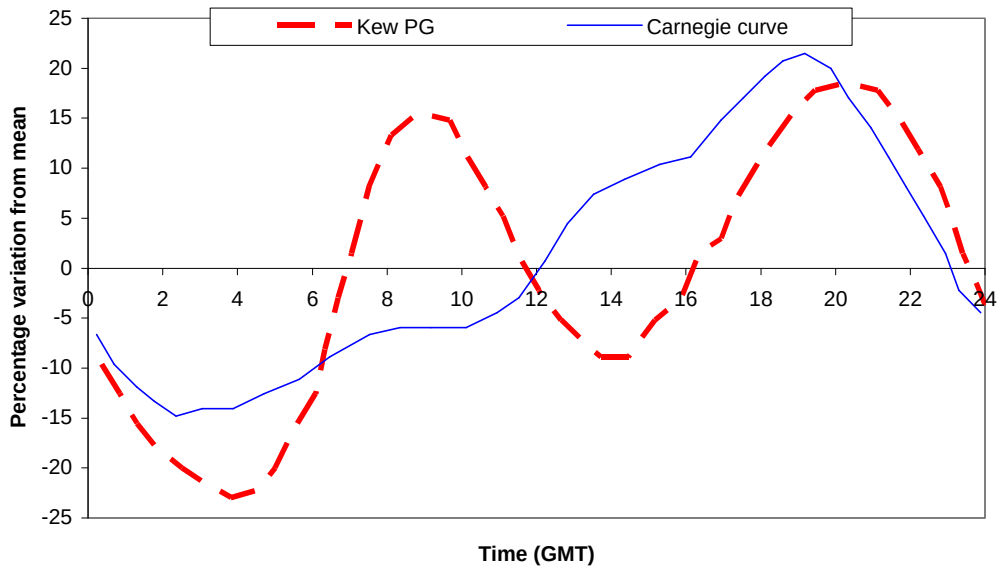

Figure 4.2. Mean diurnal relative variation of PG at Kew (1898-1931) (red dashed line) plotted with the Carnegie diurnal variation of PG over the oceans (1915-1921, 1928-1929) (blue solid line). (Adapted from Scrase, 1934).

4.2.2.2 Annual Variation

The annual variation in PG at Kew Observatory has been plotted using the original data provided by Scrase (1934) from 1898 to 1931 (figure 4.3, below). This type of variation is typical of a northern hemisphere station, where there is a maximum in the winter and a minimum in the summer (as described in section 2.4.1). Scrase (1934) comments that the gradient of the curve, in figure 4.3, from January to July is more gentle than the gradient up from July to December due to the use of domestic fires well into spring and the tendency to use fires until late autumn.

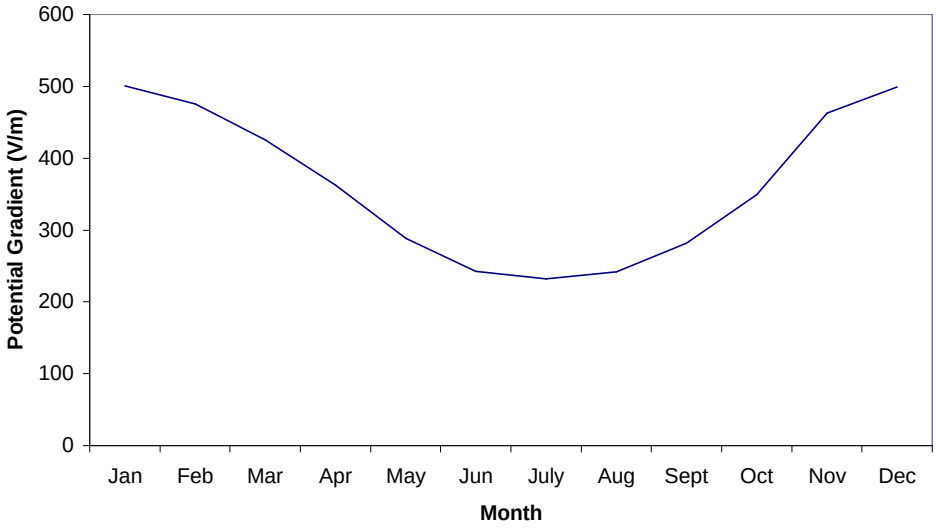

Figure 4.3. Annual variation of PG at Kew Observatory from 1898 to 1931, showing a maximum in the winter months and a minimum in the summer months. (Adapted from Scrase, 1934).

As described previously, global atmospheric electricity is controlled partly through solar activity. The Kew PG data is plotted with sunspot variation from 1898 to 1931 to highlight any possible connection between the two (figure 4.4). Scrase (1934) reports a number of hypothesis provided from Bauer (1926) and Chree (1923). Bauer (1926) suggests the sunspot period is well defined in the Kew observations in the 1913-1922 cycle. Chree (1923) argues the Kew data up to 1922 is not inconsistent with a small 11-year variation in solar activity although not to the same extent as Bauer claimed. Scrase (1934) further comments that the low PG values in 1921 and 1926 are probably due to lower pollution levels following variations in industrial activity around England in those years.

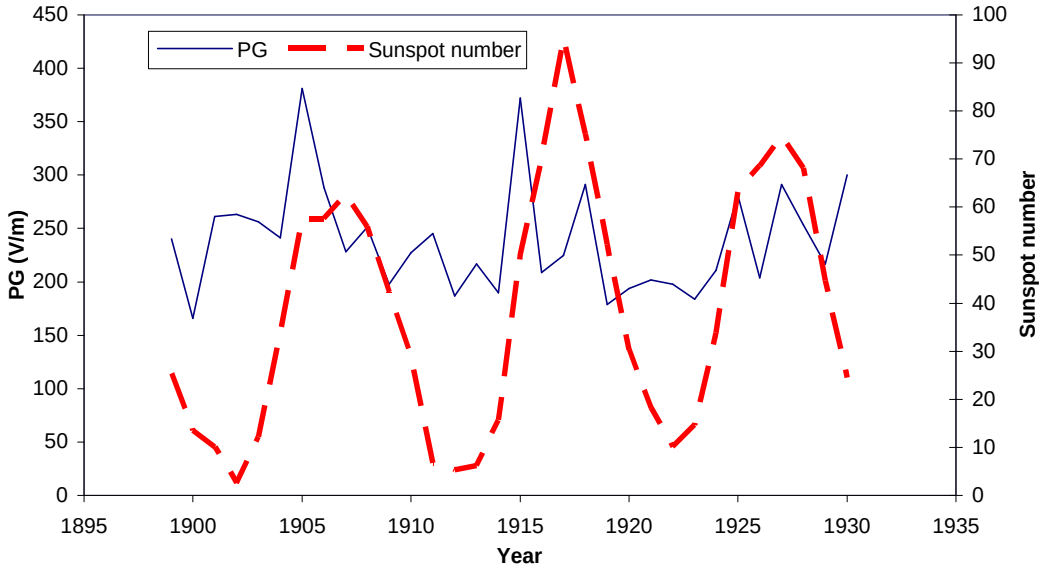

Figure 4.4. Secular variation of the PG at Kew Observatory (blue solid line) and sunspot numbers (red dashed line) in the period 1898-1931. (Adapted from Scrase, 1934)

4.2.3 PG measurements from 1861-1898

As yet there have been two sets of analysis of PG data conducted by Everett (1868) (June 1862 - May 1864) and Whipple (1881). Records of PG measurements actually exist in the period between 1877 and 1898, which have not been studied. These measurements have been taken using the Kelvin water dropper but the type of electrometer used has varied in parts of this period.

The water dropper apparatus consists of an insulated container which water flows out off in a fine stream. The point at which the stream breaks into water drops is the equalization point and each drop of water carries away a certain quantity of electricity, corresponding to its individual capacitance (Israel, 1973). A receiver is connected to an electrometer and the potential is measured. One such electrometer is the quadrant electrometer (operational during Whipple's results in 1880) where the reservoir of water is connected with the needle, keeping a fixed difference of potential between the quadrants (Chalmers, 1967). At Kew Observatory, Everett (1868) describes the original apparatus of the water dropper used. The insulated water container was housed in the observatory building with the water flowing through a brass pipe projecting through a hole in a window frame on the west end of the observatory into open air. The tip of the water dropper was approximately 11.5 ft above the ground and 3 ft away from the observatory wall. Everett (1868) explains the effect of the flow of water is to adjust the insulated water container and water pipe potential to the same electrical potential as the point in the air at which the water forms into drops.

4.3 Surface air temperature

4.3.1 Comparison between global and tropical surface air temperatures

There are a number of reasons why global or tropical temperature changes may be expected to show correlation with PG measurements which have been discussed with reference to Williams (1992, 1994) work. Studying temperature variations throughout the year in the tropics (±25^{o}) and the globe (±60^{o}), some differences can be drawn. Figure 4.5 below shows the temperature variation in the tropics and globe throughout the year.

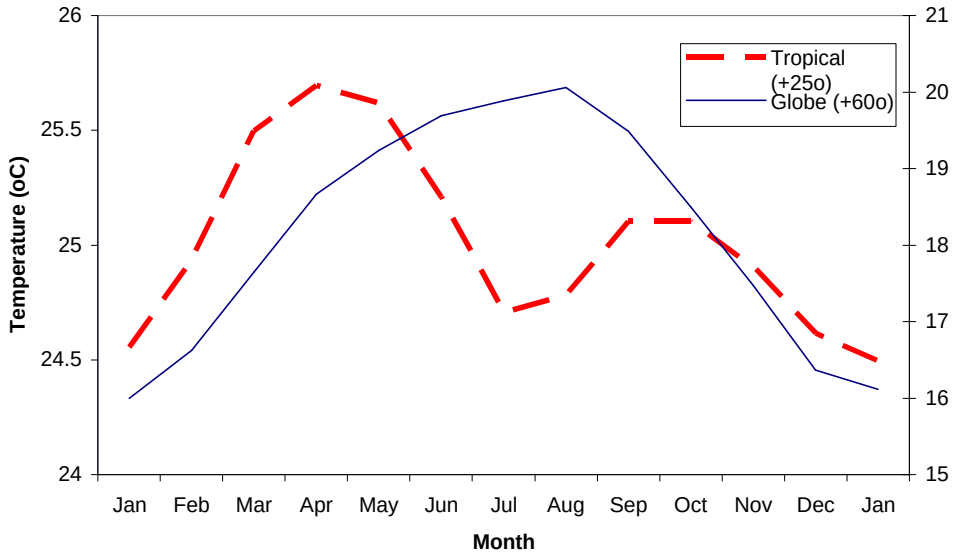

Figure 4.5. Climatological temperature variation during the year for the tropics (±25^{o}) (red line) and the globe (±60^{o}) (blue line). (Average monthly temperatures over 1961-1990). Adapted from Williams (1994).

It is clear from this figure that the mean surface air temperature in the topics has two distinct maxima in April and October. This double maxima are due to two causes; i) the slightly elliptical orbit of the earth around the sun and ii) the tilting of the earth's rotational axis with respect to the elliptical plane. The elliptical orbit of the earth around the sun produces an annual variation in solar insulation and the tilt of the earth produces a semi-annual variation as the sun crosses the equator twice each year (Liou, 1980). The global monthly variation in temperature over a year shows a single maximum in the northern hemisphere summer. Williams (1994) details Abbot's (1908) recognition that the response of surface temperature to solar insulation is strongly influenced by the ratio between land and water surface. The temperature response of land areas to insulation variations is about an order of magnitude larger than for island stations (Williams, 1994). Figure 4.6 below shows the variation in the percentage land area for the globe, through

latitudes $\pm 50^0$. It is clear from this plot that across the tropical belt ($\pm 25^o$) there is little variation in the land/sea ratio. Outside this latitudinal band, the variation is much more varied from 0 to 60%, with a smaller land ratio in the southern hemisphere and larger land ratio in the northern hemisphere. Williams (1994) suggests this is the cause of the dilution of the annual signal of surface air temperature in the tropics and for reducing the October maximum relative to the April maximum in the tropical semi-annual signal. The annual variation in global surface air temperature is therefore primarily caused by the larger land/sea ratio in the northern hemisphere.

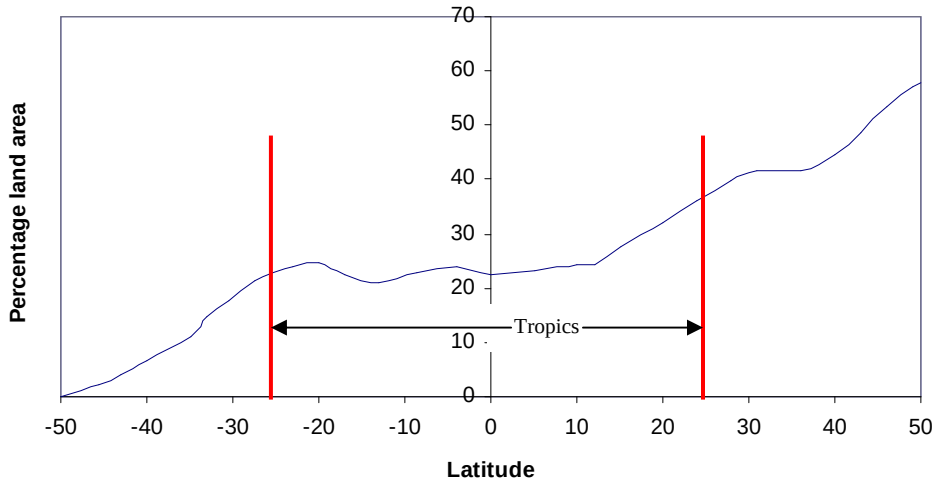

Figure 4.6. Latitudinal variation of the ratio of land to sea area for the globe. Two red lines indicate tropical band. (Adapted from Sverdrup *et al*. (1942))

An additional argument for the use of tropical temperature changes over global temperature change is the global distribution of lightning flashes. Reference is made to figure 2.2 (section 2.3) showing that approximately two of every three lightning flashes occur in the latitude band $\pm 23^o$. Evidence suggesting this can also be drawn from Optical Transient Detection plot (figure 4.7) which shows three distinct areas known as 'tropical chimney' regions. These are clearly identifiable as the dark red regions; Africa, southern N. America/northern S. America and southern Asia. It is these regions where the atmospheric electric circuit is most active and any link between the circuit and temperature should be found here.

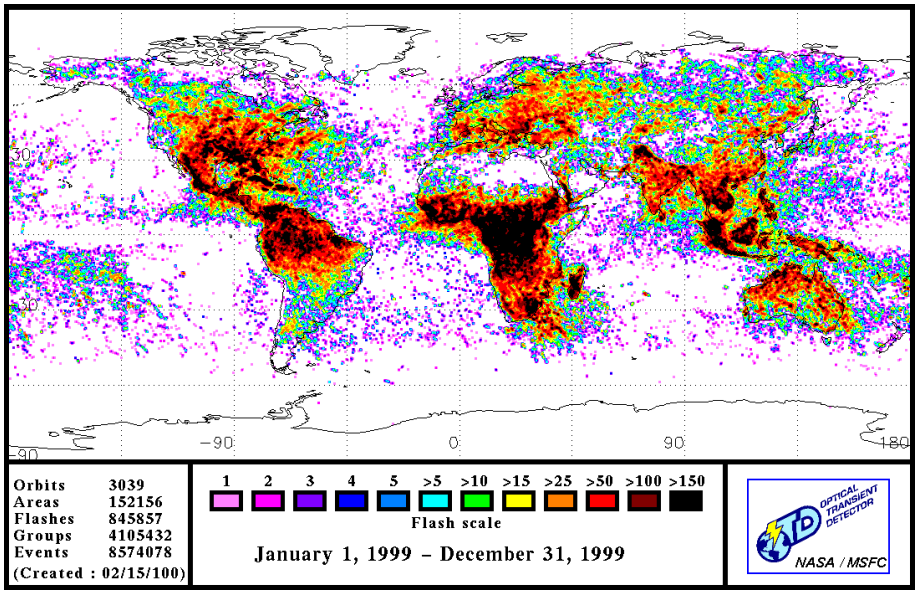

Figure 4.7. Optical Transient Detector (OTD) showing a lightning flash count ranging from 1 (light pink) to over 150 (black). This particular plot shows the annual flash count cumulative for the year 1999. Figure taken from the OTD website.

4.3.2 Observed and future changes in surface air temperature

The Intergovernmental Panel on Climate Change (IPCC) (2001) Third Assessment Report (TAR) suggests a 0.6 ± 0.2^{o}C increase in temperature has occurred since the late 19th Century. This warming has been linked with both anthropogenic and natural causes, which shall not be discussed here. Figure 4.8 below illustrates the increase in surface air temperature since 1860 to the present day. It shows two distinct warming periods; 1910 to 1945 and since 1976 with the rate of increase in both these periods being 0.15^{o}C per decade.

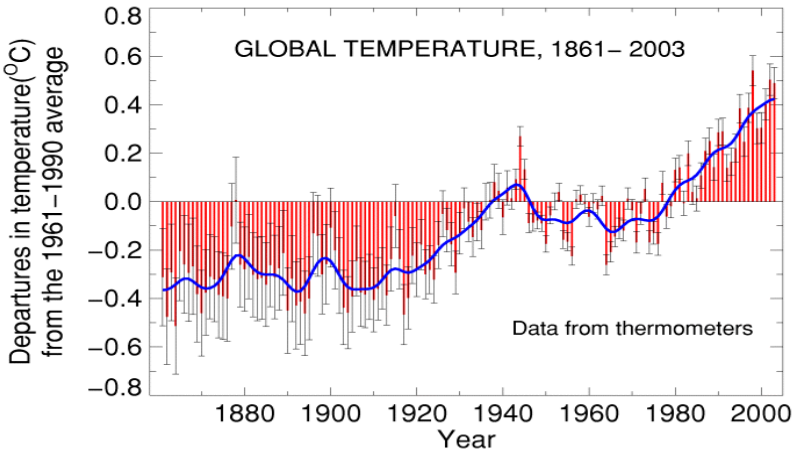

Figure 4.8. Annual land and sea surface temperature (combined) anomalies from 1861 to 2003 relative to the 1961 to 1990 average. Bars represent standard error uncertainties. (Taken from Meteorological office Hadley centre website).

The IPCC TAR (2001) states that global surface temperature is going to increase by 1.4 to 5.8°C over the period 1990-2100. This projection is estimated from the IPCC Special Report on Emission Scenarios (SRES), which uses 35 different scenarios for future projections on emissions. Using these estimated increases of global surface temperature, table 4.1 summarizes the suggested increase in lightning frequency by Williams, 1992 and 1994, Price and Rind, 1994 and Reeve and Toumi, 1998. As seen the largest sensitivity is provided by Reeve and Toumi, 1998 which calculates to a possible 232% increase in lightning activity over the period 1990-2100 if global temperatures rise by 5.8°C.

Table 4.1 – Summary of change in lightning frequency with global surface temperature changes reported by the IPCC TAR (2001) as suggested by authors listed in the first column. All figures represent an increase in lightning frequency for the period 1990-2100.

	1.4°C rise	**5.8°C rise**
Williams, 1992	14.7 fold	61.1 fold
Williams, 1994	14%	58%
Price and Rind, 1994	7.7%	31.9%
Reeve and Toumi, 1998	56%	232%

Surface air temperature data used in this dissertation is obtained from the Meteorological Office's Hadley Centre. There is a continuous data series of surface air temperature from 1870 to the

present day. The temperature record is presented as monthly average anomalies from the 1961-1990 average and is segmented into regional categories as well as global anomalies i.e. tropical temperature anomalies can be obtained.

Chapter 5 – Exploratory analysis of Kew PG data in the period 1939-1950

5.1 Introduction

The original records of uncalibrated PG data between 1876 and 1898 are currently at the National Meteorological Archives in Bracknell, UK. The records are strips of the original photographic traces of electrometer deflection. From evidence provided on the photographic strips they were changed at approximately 1050 GMT every two days allowing for one complete 24-hour diurnal cycle on one chart (an example of the photographic trace can be seen in figure 5.1). As the data is not calibrated to an absolute measure of PG, exploratory data analysis is used to determine a calibration that can result in an absolute value of the global electrical signal. Calibrated data from 1939-1950 is used as a tool in this preliminary analysis and will be used to investigate an absolute calibration for the relative PG values in the 1877-1898 data.

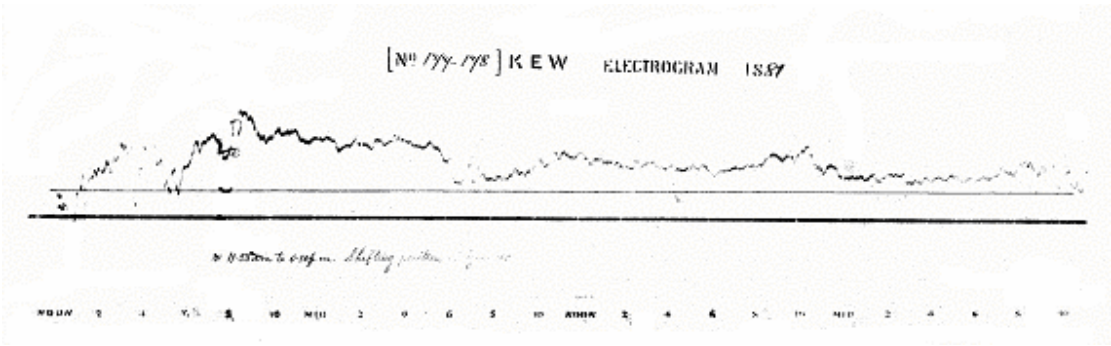

Figure 5.1 – Showing an example of the original photographic electrogram from 1043 GMT on June 25 1881 to 1110 GMT on June 27 1881 at Kew Observatory.

5.2 Method of analysis

There are a number of possible approaches to find an absolute PG calibration. The first would be to completely re-model the electrometer and landscape at Kew Observatory. This would allow relative measurements to be made alongside absolute measurements of PG and a calibration factor found. However, this method could not be used as the landscape at Kew Observatory has changed since 1861 through to its closure in 1981 (Scrase, 1934) and exposure of the electrometer would influence the measurements made. The second method is to assume the mean PG has not changed in the last two centuries. This allows easy comparisons to be made between all data sets of PG at Kew and around the world. This method assumes the global electric circuit remains constant and no local factors influence the PG. This method would not be accurate as Harrison (2003b) reports that long-term global electric circuit measurements have reduced in the 20th century and local

factors can strongly influence the PG. The final method that is used here is an absolute calibration of the original data using known calibrated measurements of PG from 1939 - 1950.

As the Kew record is continuous from 1876 to 1898, there are potentially approximately 8,400 days of record that can be used. An appropriate month and time in the day is found from investigation when of the local pollution effects on the PG data is at a minimum. This enables selection of days and times when a global signal could dominate. This is investigated in section 5.3. Five different calibration methods have been considered using a limited amount of data, which will be compared and are explained in section 5.4. A summary of the process in achieving a suitable calibration is shown in a flow diagram (figure 5.2).

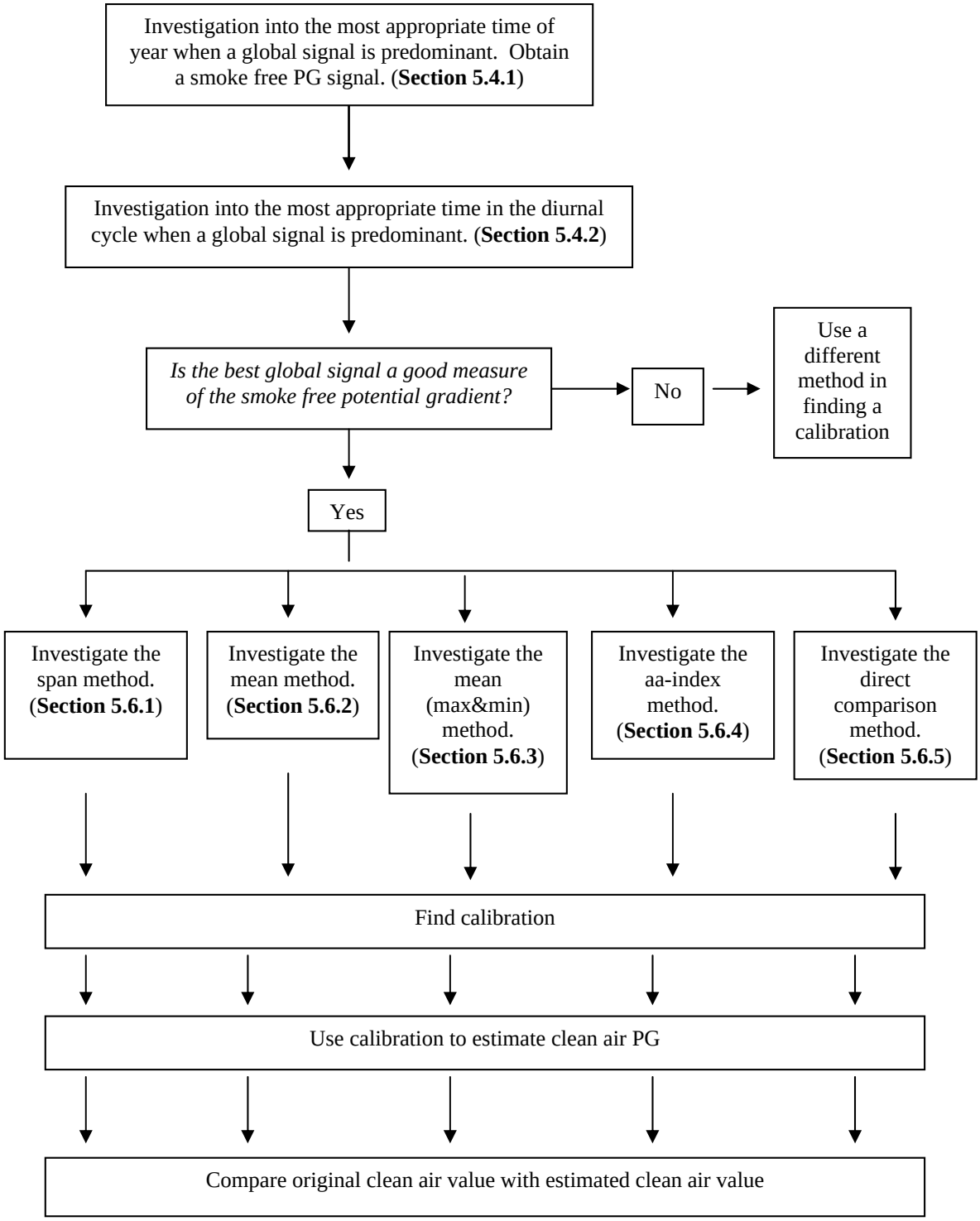

Figure 5.2. Flow chart showing the methodology adopted in finding an appropriate calibration from 1940-1950 PG data to be used on uncalibrated PG data between 1877 and 1898.

5.3 Investigation into annual and diurnal cycle

To establish the best time in the year and day when a global signal of atmospheric electricity may be dominant at Kew Observatory, the local effect of pollution on PG is investigated. Smoke pollution was measured and recorded at Kew Observatory during the same period as the PG data used in this analysis (1939-1950). The smoke pollution data can be correlated with PG measurements to investigate a possible link and establish when the smoke pollution has the least effect on PG.

5.3.1 Annual cycle in PG at Kew between 1939 and 1950

Figure 4.3 in section 4.2.2.2 showed the annual variation of PG at Kew with maximum PG in winter and minimum PG in summer. Comparison of the average hourly PG difference from the summer (May, June, July, August) and winter (November, December, January, February) means with actual smoke pollution values for the same time during the day is made. Figure 5.3 (a) and (b) show an example of such a comparison in 1939. These plots indicate a high positive correlation of PG and smoke pollution in the winter months (correlation coefficient, r of 0.94) and a lower positive correlation in the summer (r = 0.68). By using Ordinary Least Squares linear regression, the PG can be extrapolated to zero smoke – the equivalent 'clean air PG', which becomes useful in later analysis. A summary of the correlation coefficient and equivalent clean air PG values for each the summer and winter plots between 1939 and 1950 is shown in table 5.1.

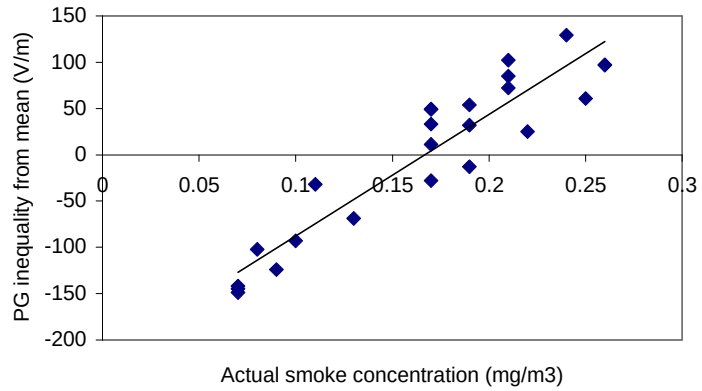

(a) - Winter

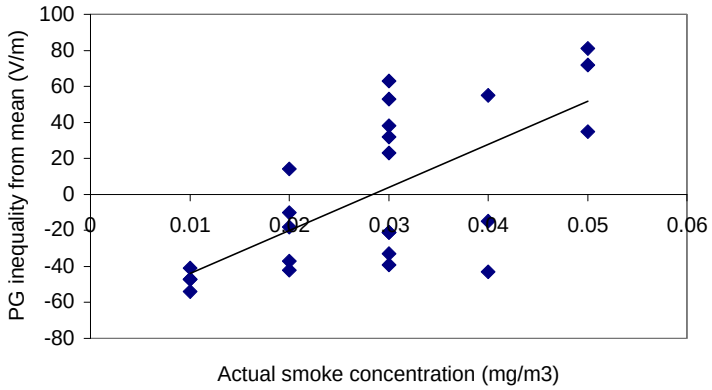

(b) - Summer

Figure 5.3. Average diurnal PG inequality from mean PG in (a) winter and (b) summer against the actual diurnal smoke concentrations for 1939 at Kew Observatory.

Table 5.1 Summary of the correlation coefficient (r) and equivalent clean air PG values from the average diurnal PG inequality from mean in winter and summer against the actual diurnal smoke concentrations.

		r	Equivalent clean air PG (V/m)
1939	Summer	0.68	218
	Winter	0.94	265
1940	Summer	0.77	103
	Winter	0.94	248
1941	Summer	0.81	105
	Winter	0.92	259
1942	Summer	0.71	189
	Winter	0.91	235
1943	Summer	0.82	132
	Winter	0.91	313
1944	Summer	0.67	179
	Winter	0.85	310
1945	Summer	0.60	178
	Winter	0.92	250
1946	Summer	0.80	198
	Winter	0.94	332
1947	Summer	0.75	173
	Winter	0.93	198
1948	Summer	0.76	169
	Winter	0.82	217
1949	Summer	0.70	209
	Winter	0.88	294
1950	Summer	0.94	177
	Winter	0.75	374

Studying the correlation values (r), the average for winter months is 0.91 and the summer is 0.73. This indicates that in the winter the PG measured is most strongly influenced by the smoke concentration in the local area with less of the variability in summer due to smoke. Figures 5.4 (a) and (b) below shows the variation of equivalent 'clean air' PG for each season from 1939-1950. The actual mean PG is also shown in figures 5.4 (a) and (b) to illustrate that the difference in PG between the actual mean and equivalent 'clean air' in the summer is lower than the winter – providing further confidence that the equivalent 'clean air' PG in the summer is a better measure of actual PG than in the winter. The plot also highlights the result that summer months show a lower PG than the winter months. For further validation that the equivalent 'clean air' PG as estimated by smoke free conditions at Kew, PG data from Eskdalemuir, Scotland ($55^{o}19$'N, $3^{o}12$'W) is also plotted in figures 5.4 (a) and (b).

Eskdalemuir is considered to be an ideal site for measuring the global PG signal and provides useful for inferring variations in the global atmospheric electrical circuit (Harrison, 2004). Both the equivalent 'clean air' PG and the Eskdalemuir PG show similarities in the trend, though the trends in the winter months are more similar than in the summer months (fig 5.4). It is apparent that there is variability of PG in the summer with a more stable PG in the winter. Combining the summer and winter months, the Eskdalemuir PG is on average 49 V/m smaller than the Kew PG.

Focusing on the summer months in plot (a), the Eskdalemuir PG is an average 33 V/m smaller than the estimated equivalent 'clean air' at Kew.

So there are three reasons to consider the summer PG as having the lowest smoke contribution; (i) there are lower absolute values of PG in the summer, (ii) there is less variability explained by the smoke data in the summer (iii) clean air PG from Eskdalemuir shows very similar variations with estimated clean air from Kew. It is now necessary therefore, to further investigate the summer months in finding a time in the diurnal cycle when the possibility of a global signal is present.

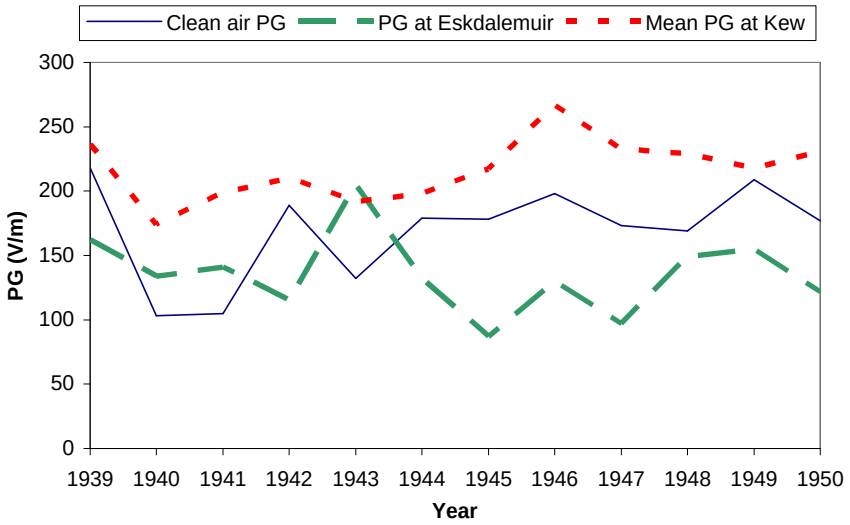

(a) - Summer

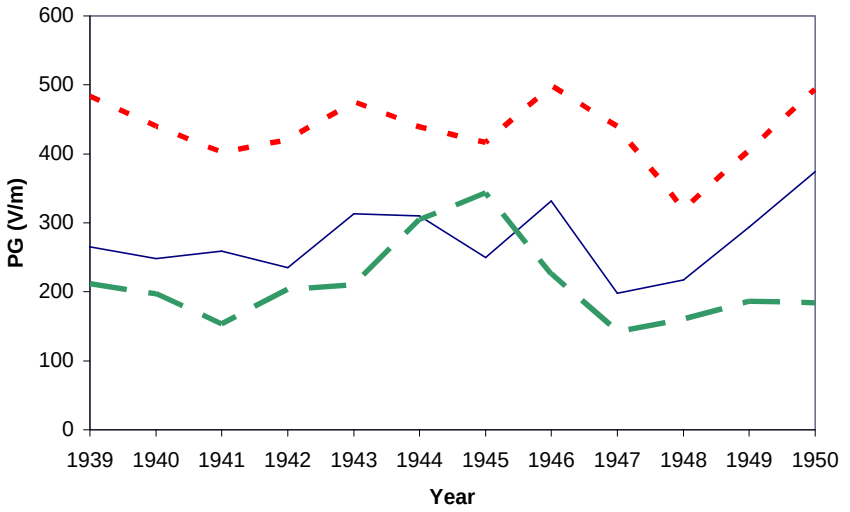

(b) - Winter

Figure 5.4. Plot showing the variation in the equivalent 'clean air' PG (blue solid line), the mean PG (red small dash line) and PG from Eskdalemuir (green large dash line) throughout the period 1939-1950 in the (a) summer months and (b) in the winter months.

5.3.2 Diurnal cycle of PG at Kew between 1939 and 1950

It has been shown that the summer months are the most likely months when a global signal of PG is most likely. Further analysis is conducted to investigate an optimum time in the diurnal cycle when the PG is most predominant. It is necessary first, to obtain a value of PG that could be closest in representing the clean air (smoke free) value as shown in table 5.1. Figure 5.5 below shows the average diurnal cycle for the years 1939-1950. Studying this plot and analysis of the summer average diurnal cycle indicates that in 50% of the years (1939-1950) the minimum PG occurs at roughly 1430 UT with 25% of cases occurring at roughly 1530 UT.

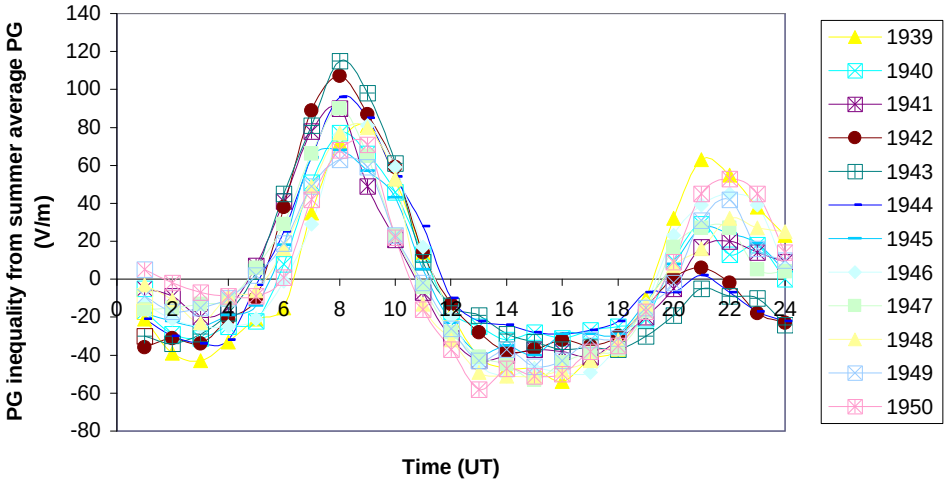

Figure 5.5. Plot showing the summer average diurnal cycle for all years between 1939 and 1950. PG measurements are plotted as the difference in the summer average PG.

However, comparison of the minimum PG at each hour shows the largest correlation with equivalent 'clean air' PG (from table 5.1) occurs at 1830 UT. On closer inspection of the PG at 1830 UT, it appears that this is the time when the PG is close to the mean value PG in the day. Highlighting it as the time when the global signal is significant would be inappropriate because the mean PG is a measure of the whole 24 hours in a diurnal cycle, suggesting the whole period represents a global signal of PG – this is incorrect as it has previously been suggested that a global signal is most dominant when the PG is lowest. Figure 5.6 below shows a positive correlation (r = 0.52) between the minimum PG at 1430 UT and the estimated clean air value.

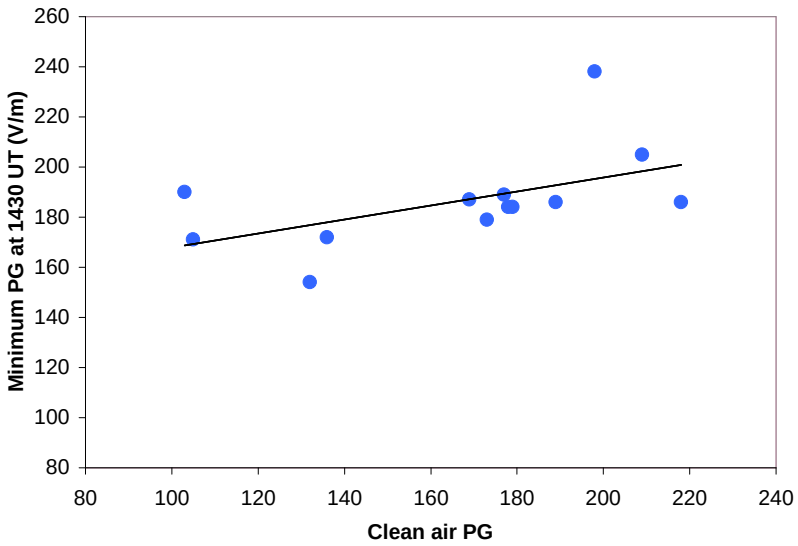

Figure 5.6. Correlation between the estimated clean air PG (from table 5.1) and the minimum PG occurrence at 1430 UT in the summer months for years 1939-1950.

This shows that the most likely period when the local effects of pollution at Kew have the least effect on the PG measurements is in the summer at approximately 1430 UT.

5.4 Calibration methods

Below is a description of the five different methods in finding an absolute calibration using data from 1939-1950.

i) A measure of the diurnal span from the time when the global signal might be present (1430 UT) with the maximum and minimum values. This will require the recording of three points on the diurnal cycle of PG (see figure 5.7). This method will be referred to as the *Span method* and is calculated using equation 5.1

$$C_{span} = \frac{Y_{global}}{Y_{\max} - Y_{\min}} \qquad \textbf{(5.1)}$$

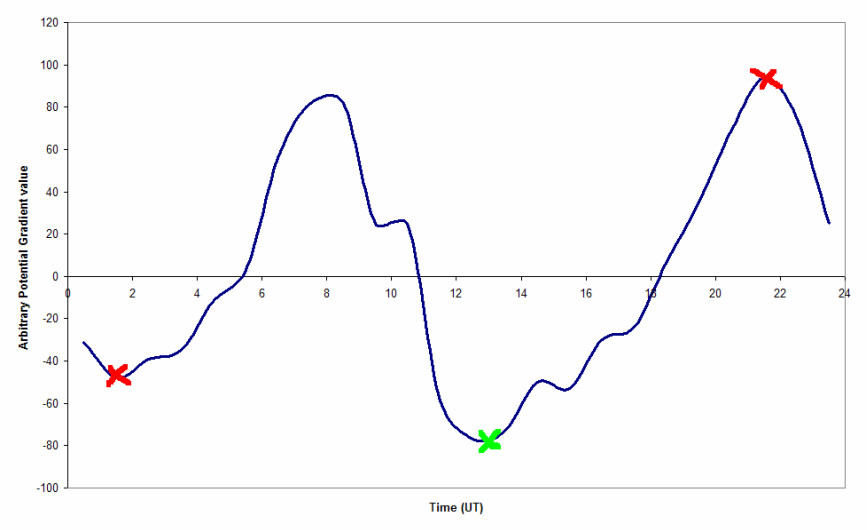

Figure 5.7. Example of the average summer diurnal cycle in 1939 showing the required points needed for the coefficient of the span. Green cross represents the 1430 UT global signal PG and red crosses represent the maximum and minimum values; the span of values.

ii) A measure of the global signal value with the mean calculated from an average of the maximum and minimum values. Three points will be required on the diurnal cycle (see figure 5.8). This will be referred to as the *Mean (max&min) method* and is calculated using equation 5.2. This method is used to determine a coefficient of the mean by obtaining a small collection of values while still trying to achieve a significant calibration coefficient. It follows from the standard meteorological approach to calculate the mean diurnal temperature by averaging the maximum and minimum daily temperatures. In this particular method, the global signal value is recorded with the average maximum and minimum values.

$$C_{mean(\max\&\min)} = \frac{Y_{global}}{\frac{1}{2}\left(Y_{\max} + Y_{\min}\right)} \qquad \textbf{(5.2)}$$

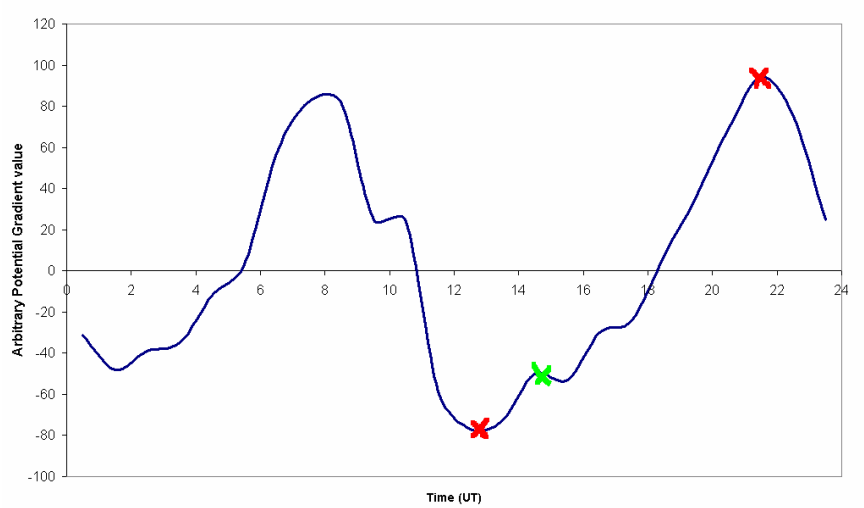

Figure 5.8. Example of the average summer diurnal cycle in 1939 showing the required points needed for the coefficient of the mean using the average of maximum and minimum values. Green cross shows the probable global signal value and red crosses represent the maximum and minimum values.

iii) A measure of the global signal value with the actual mean diurnal variation throughout the day. This requires a total of roughly 24 recordings (i.e. once every hour throughout the day) and will take a much longer time than (ii), which is not desirable. Referred to as the *Mean (actual) method*. This follows the same method as the previous (ii) but takes an average of the whole diurnal cycle instead of the mean estimated from the maximum and minimum value and is calculated using equation 5.3 below. This method is investigated to establish how well calculating the mean by using the maximum and minimum values, by comparing results using the actual mean coefficient.

$$C_{mean(actual)} = \frac{Y_{global}}{Y_{mean}} \qquad \textbf{(5.3)}$$

iv) A coefficient using the mean diurnal PG (calculated from the maximum and minimum values) and a measure of the geomagnetic *aa*-index. The *aa*-index is related to cosmic ray activity which in turn modulates the atmospheric electrical system. More specifically, the *aa*-index is a measure of the average solar magnetic activity at two antipodal[4] subauroral stations; Hartland, UK and Canberra, Australia (*Mayaud*, 1972). *Harrison and Aplin* (2002) used the *aa*-index to calibrate Kew PG data. *Mayaud* (1972) showed the *aa*-index to vary in phase with solar activity indicators such as

[4] Countries on opposite sides of the globe.

sunspot number during the 19th century and that it is an inverse proxy for cosmic rays. This coefficient is calculated using equation 5.4 below.

$$C_{aa-index} = \frac{Y_{global}}{\left(aa - index \Big/ \left[\frac{1}{2} \left(Y_{\max} + Y_{\min} \right) \right] \right)} \quad \textbf{(5.4)}$$

v) A direct comparison of original records from 1940-1945 and the known PG values. By obtaining the relative values from 1940-1945, a relationship is found between these and the known tabulated PG values. This relationship is used to calculate a scale value of PG, which is then used in the *aa*-index method (iv) above to find the *aa*-index coefficient.

In order to establish which of the five methods would be the most suitable, an assumption is made that the already known calibrated data from 1939-1950 are arbitrary values with no reference to volts per metre. Each of the five methods is then used to calculate a calibration to PG values. These can then be validated by correlation with the known clean air PG values.

5.5 Results

5.5.1 Span method (C_{span})

By applying this methodology to all years between 1939 and 1950, a data set of span coefficients is plotted with the equivalent clean air PG values (from table 5.1) giving a linear regression. This linear regression is used in the form shown in equation 5.5 to calculate a clean air PG as calibrated using the span method.

$$\textit{Calibrated clean air PG} = (-5.1145 \times C_{span}) + 146.85 \quad \textbf{(5.5)}$$

Using the linear regression model to calculate the clean air PG a comparison can be made with the original calibrated clean air PG as validation. A plot of this is seen in figure 5.9. The correlation coefficient is 0.26, which as the best fit line shows, is a poor correlation.

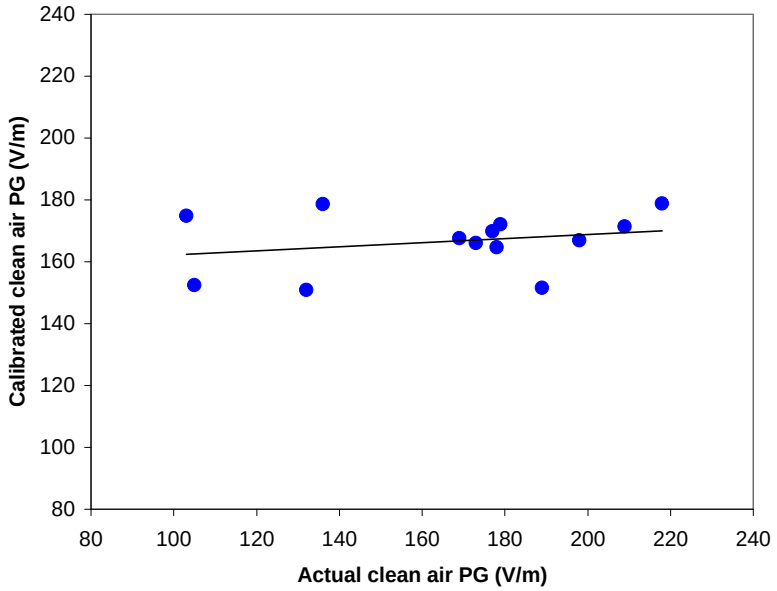

Figure 5.9. Span method calibrated clean air PG with the actual clean air PG for all years between 1939 and 1950.

5.5.2 Mean (max and min) method ($C_{mean(max\&min)}$)

As with the span method explained above, the coefficient is found for each year and is compared with the original calibrated clean air PG values. This gives a linear regression fit and is used in the form of equation 5.7 to calculate the calibrated clean air PG.

$$Calibrated\ clean\ air\ PG = (-0.0355 \times C_{mean(max\&min)}) + 156.93 \qquad \textbf{(5.7)}$$

As in the previous, the calibrated clean air PG using this method is correlated with the original calibrated clean air PG and can be seen in figure 5.10. This shows a correlation coefficient of 0.24, which is not a significant correlation between the two data sets.

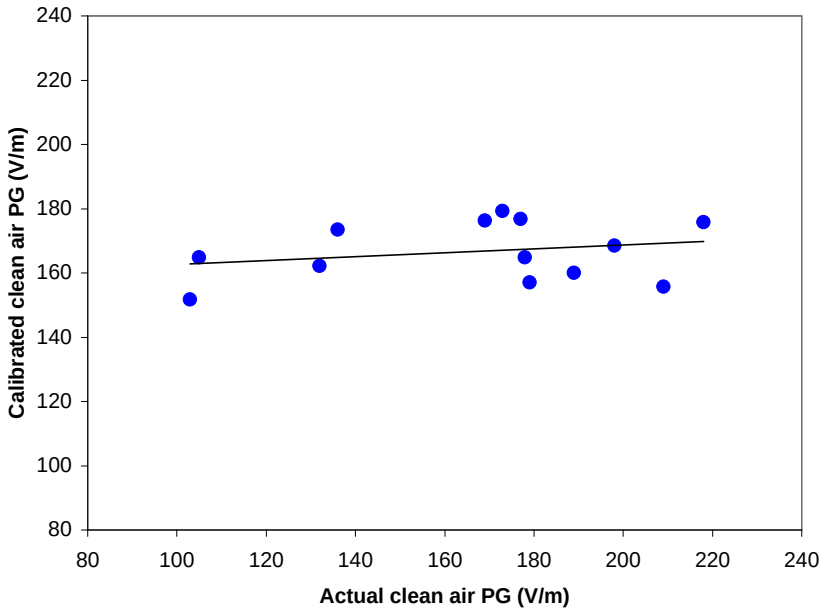

Figure 5.10. Mean (max&min) calibrated clean air PG with the actual clean air PG for all years between 1939 and 1950.

5.5.3 Mean (actual) method ($C_{mean(actual)}$)

The coefficient is found for each year and compared with original clean air value and the linear regression model is shown in equation 5.8.

$$Calibrated\ clean\ air\ PG = (-1.9185 \times C_{mean(actual)}) + 153.16 \quad \textbf{(5.8)}$$

Once again, the calibrated clean air PG from equation 5.7 is compared with the original clean air PG (table 5.1) and is illustrated in figure 5.11 below. For this plot, the correlation coefficient is 0.24. Again, this represents a poor correlation between the calibrated clean air PG and the actual calibrated values and shows there is not much improvement in using 24 points in finding the mean over the maximum and minimum method.

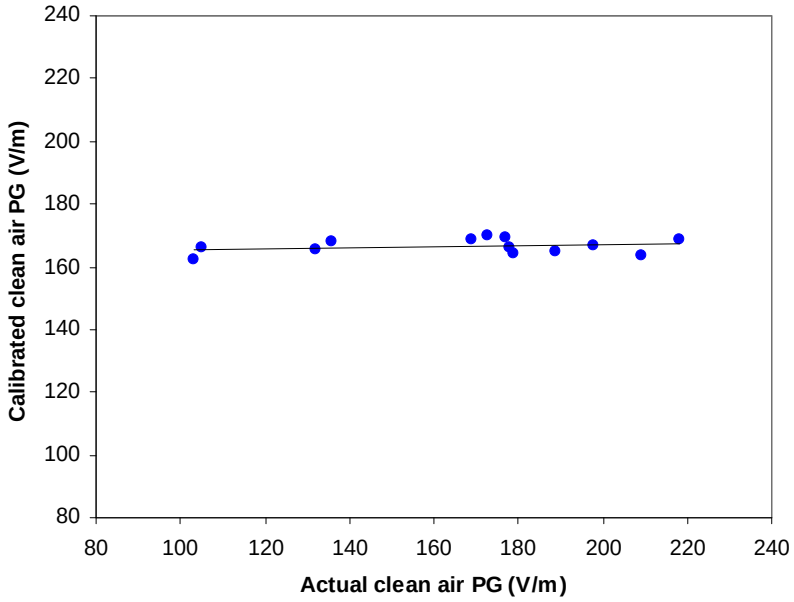

Figure 5.11. Actual mean calibrated clean air PG with the actual clean air PG for all years between 1939 and 1950.

5.5.4 Geomagnetic aa-index method ($C_{aa\text{-}index}$)

Using the *aa*-index as a method for determining a calibration, a comparison is firstly made between the estimated clean air PG (from table 5.1) and the coefficient of the *aa*-index with the mean (using the maximum and minimum to calculate the mean). The plot in figure 5.12 below shows a significant positive correlation (r = 0.56 for 13 values) assuming the values are independent of each other.

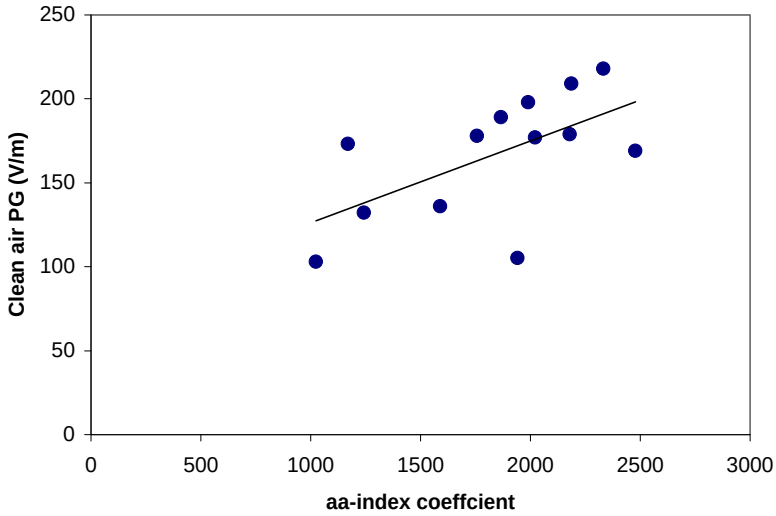

Figure 5.12. Correlation of the yearly averaged surface clean air PG and the *aa*-index coefficient (as calculated using equation 5.4) for the same period (1939-1940)

Using the linear relationship in figure 5.13 in the form shown in equation 5.8 below, the calibrated clean air PG can be calculated for validation.

$$\textit{Calibrated clean air PG} = (0.0489 \times C_{aa\text{-}index}) + 77.214 \qquad \textbf{(5.9)}$$

Using the *aa*-index calibration, the calibrated clean air PG is calculated and is correlated with the original calibrated clean air PG. This can be seen in figure 5.13 below and clearly shows a positive correlation between calibrated and actual clean air values. The correlation coefficient is 0.6, which is a significant positive correlation in the 95% confidence interval (for 13 independent points).

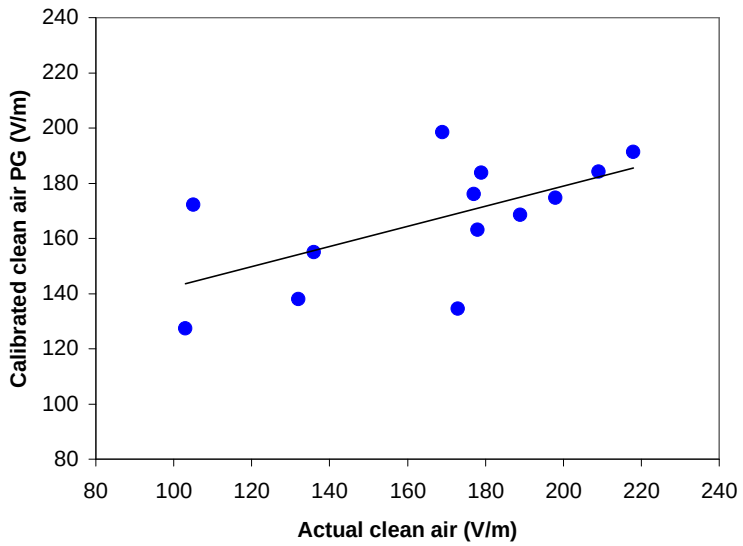

Figure 5.13. *aa*-index coefficient of mean calibrated clean air PG with the actual clean air PG for all years between 1939 and 1950.

5.5.5 Direct comparison of original record with known PG values

By obtaining relative measurements from years where the PG is already calibrated and tabulated a direct relationship has been found between the two. Table 5.2 below shows the relative values and calibrated values at four points (0730, 1430, maximum and minimum) during the diurnal cycle for 1940-1945.

Table 5.2. June averaged PG values both calibrated and relative values for the years 1940-1945.

	Calibrated PG (V/m)				Uncalibrated PG			
	0730	**1430**	**Max**	**Min**	**0730**	**1430**	**Max**	**Min**
1940	245	139	245	101	21.7	16.0	24.0	13.0
1941	289	171	295	147	26.0	18.4	28.6	17
1942	302	159	302	153	33.67	18.0	35.7	17.6
1943	271	149	273	145	20.4	17.9	20.6	18.2
1944	231	177	231	155	24.3	15.3	24.6	16.3
1945	227	130	227	126	22.1	14.2	22.6	12.1

Figure 5.14 below shows a plot of the correlation between the calibrated and relative values for each of the years. The average correlation coefficient for all these correlations is 0.95. This indicates a significant relationship (for 4 values) between the two and shows that the relative values can be explained by the calibrated values.

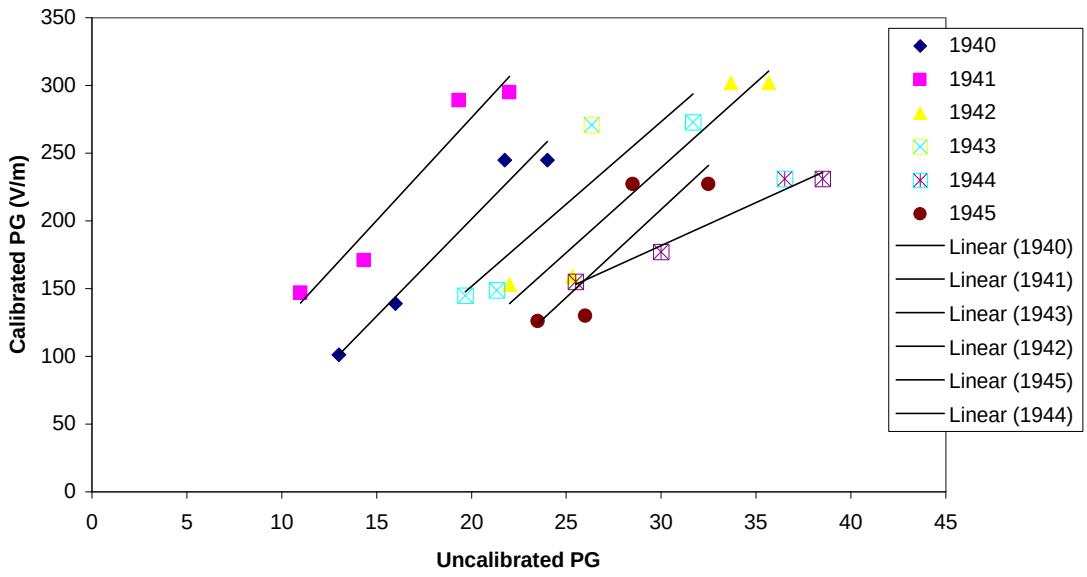

Figure 5.14. Correlations between calibrated and relative PG values averaged for June in the years 1940-1945, for 4 points selected each day (1430 UT, 0730 UT, max and min).

The linear relationship expressed in each year can be averaged to obtain a relationship in the form shown in equation 5.9 below. This relationship is used on the relative values and a value that can then be used in the *aa*-index method to find a comparable PG is found and compared with calibrated PG.

$$\textit{Scaling value of PG} = (9.4787 \times \textit{relative measure of PG}) + 6.932 \qquad \textbf{(5.9)}$$

For validation, the calibrated PG and known clean air PG are correlated as shown in figure 5.15. The correlation coefficient for this relationship is 0.63 which represents a good correlation.

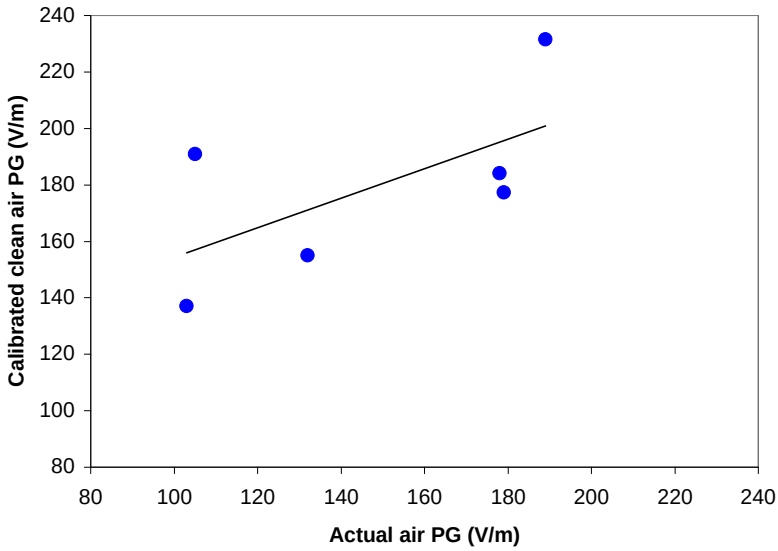

Figure 5.15. Plot showing the calibrated clean air PG correlated with the equivalent clean air PG. Values are for 1430 UT averaged in June in each year from 1940-1945

5.6 Conclusion to exploratory data analysis

The coefficient of determination for each of the methods used in the preliminary analysis is shown in ascending order of usefulness in table 5.3 below.

Table 5.3. Summary table of the most appropriate coefficient method for calibration.

Method	**Correlation coefficient**
Direct comparison with *aa*-index	0.63
aa-index	0.60
Span	0.26
Actual mean	0.24
Mean (max and min)	0.24

This highlights the best method in calibrating the PG data is the *aa*-index method using a scale value as estimated from a direct comparison from known PG with relative PG (between 1940-1945). This result means that there are three necessary values from the 1876-1898 PG record at the National Meteorological Archive in Bracknell; 1430 UT, maximum and minimum in the month of June.

It must also be highlighted here that the days selected must also be fair-weather days i.e. no disturbed activity such as thunderstorms, rain or fog. These days can be selected when the PG trace does not drop below zero and when there are no erratic changes in the traces. Figures 5.16 (a) and (b) show examples of such a trace where (a) shows a fair-weather day and (b) a disturbed weather day. The aa-index for the period 1876-1898 is also obtained for use.

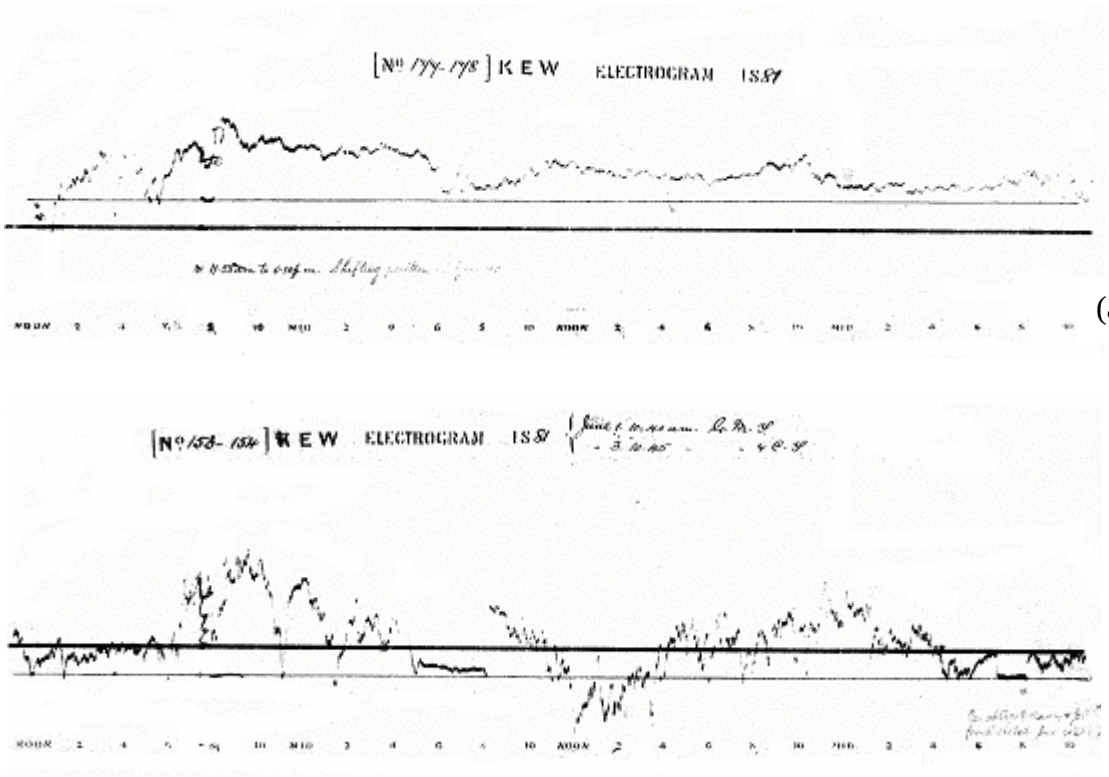

(a)

(b)

Figure 5.16. Two original electrographs from June 1881. (a) runs from 10:43am on 25th June 1881 to 11:10am on 27th June 1881 and shows a typical 'fine-weather' day. (b) runs from 10:40am 1st June 1881 to 10:45am on 3rd June 1881 and shows a disturbed weather day.

Chapter 6 – Analysis of new PG data from 1877-1932

As explained in chapter four and five, the original Kew Observatory PG records for the period 1877-1898 are held at the National Meteorological archive in Bracknell, UK, which have not been previously analysed. Using the direct comparison with *aa*-index method (section 5.6.5) for calibration, the raw data is calibrated accordingly. Section 6.1 outlines some difficulties in the collection of raw data from the archive with some interesting findings from the early data. The calibrated data is discussed in section 6.2 with early observations noted before comparisons of global and tropical temperature changes with the PG measurements from 1877-1932.

6.1 Raw measurements of PG

6.1.1 Instrumental and data record

Part of the initial aim of the dissertation was to calibrate relative values of PG from 1877-1898, however, inevitable problems are associated with very early records. The continuous record of PG was found to start in April 1874, with the first full year beginning in 1875. It was found that these very early records were either damaged considerably or had no time series recorded on the original photographic paper for any data collection. Although records for 1876 were reasonably in tact and contained detailed notes of events (such as when the photographic paper was changed, times when the water-dropper tank was filled and meteorological observations) the majority of photographic traces had no time series and did not meet the criteria as set out in chapter five, section 5.4. Figure 6.1 below shows an example of one of the earliest photographic traces.

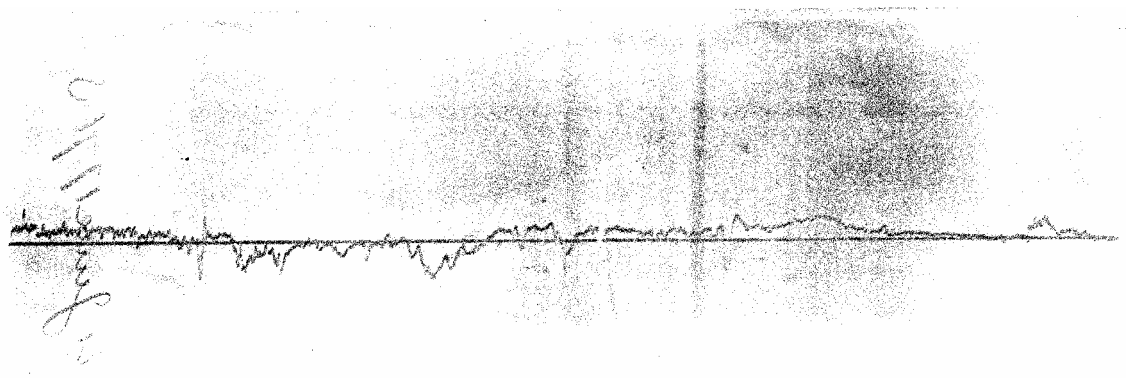

Figure 6.1. Photographic trace of PG variations from the Thomson water-dropper electrometer at Kew Observatory on 13th June 1876.

Throughout the time period of collection, other problems and complications existed in the records such as:

- Wind up clock for the electrometer stopping.
- No zeroing occurring in some years
- Water-dropper tank left empty for a number hours in the day
- Zero position shifting
- Objects such as a cloth being left on the electrometer, disturbing the PG

Data was not obtained in June 1886 as for some unknown reason the record was missing for this time. Another notable occurrence at the observatory was a fire on 2nd September 1887, which put the observatory out of action until February 1888. During this time, the observer noted the silver battery was re-charged and a new case was fitted to the instrument. During this time, experiments were also conducted to find an absolute calibration for the electrometer. Results of the experiments were not noted. Other calibration experiments were conducted in 1893 where the results were scribed on the side of the photographic paper for the period 31st May to 2nd June. This scale was not repeated after that.

6.2.2 Relative PG data

To obtain relative values of the PG from the photographic strips, the author of this study used transparent graph paper that was aligned with the zero line (or a reference line with no presence of zeroing). From here, the 1430 UT, maximum and minimum values were recorded by measuring the height of the PG trace. The recorded relative values are shown in tabulated form in appendix one.

Table 6.1. (a) June averaged raw data of PG at Kew Observatory from 1887-1898. (b) aa-index values obtained from the Institute de Physique du Globe de Paris website. The original data can be found in appendix 1.

(a)

	No. days in average	1430	Max value	Min value
1877	1	17.0	23.0	10.0
1878	4	19.0	43.0	11.8
1879	5	15.6	31.6	11.6
1880	4	20.0	44.3	13.5
1881	5	16.4	35.1	11.6
1882	2	18.5	40.0	4.0
1883	2	15.5	31.0	0.5
1884	3	30.3	52.7	13.0
1885	3	22.7	61.3	0.3
1886	------	------	-----	-----
1887	4	14.8	28.8	10.5
1888	3	16.7	31.6	12.0
1889	3	23.0	31.3	10.7
1890	2	14.0	27.0	12.5
1891	5	21.2	31.0	18.0
1892	3	19.0	37.7	11.7
1893	1	16.0	21.0	14.0
1894	4	19.0	26.5	14.8
1895	3	24.7	35.7	19.3
1896	2	16.5	30.0	11.0
1897	5	21.8	75.2	17.2
1898	4	18.5	40.8	15.0
Average	*3.2*	*19.1*	*37.1*	*11.6*

(b)

aa-index
8.9
8.6
5.9
7.3
10.7
19.0
18.5
13.1
14.2

12.6
14.5
9.9
7.3
11.7
17.7
17.1
20.0
17.6
11.7
12.0
14.3

Table 6.1 above shows the June averaged relative values of PG at the most significant times in the diurnal cycle as discussed in chapter five along with the *aa*-index value for the same period. These values are used to determine calibrated global PG measurements by using a combination of the direct comparison and *aa*-index method (chapter five). Equations 6.1 to 6.3 below are used in order they are shown to obtain the calibrated data set as seen in table 6.2.

$$\textit{Scaling value of PG} = (9.4787 \times \textit{relative PG}) + 6.932 \qquad \textbf{(6.1)}$$

$$C_{aa-index} = \frac{Y_{global}}{\left(aa-index \Big/ \left[\frac{1}{2} \left(Y_{\max} + Y_{\min)} \right) \right] \right)} \qquad \textbf{(6.2)}$$

$$\textit{Calibrated clean air PG} = (0.0489 \times C_{aa\text{-}index}) + 77.214 \qquad \textbf{(6.3)}$$

N.B. Y_{global}, Y_{max} and Y_{min} represent the 1430, maximum and minimum values in table 6.1 (a) respectively.

A table of the calibrated PG at Kew Observatory using equations (6.1)-(6.3) above is shown below (table 6.2). Figure 6.2 below shows a time series plot shows of the newly calibrated PG measurements from 1877-1898 and other calibrated measurements at Kew from 1898-1931. (1898-1931 PG measurements obtained from Scrase (1934))

Table 6.2. June averaged calibrated PG measurements in Volts per meter from 1877-1898

	PG (V/m)
1877	227.4
1878	348.2
1879	344.6
1880	428.3
1881	242.5
1882	175.2
1883	141.2
1884	400.1
1885	292.1
1886	-----
1887	186.5
1888	193.4
1889	296.7
1890	258.5
1891	275.7
1892	196.8
1893	155.3
1894	167.2
1895	245.6
1896	212.2
1897	436.5
1898	239.0

Figure 6.2 below shows a negative trend in global atmospheric PG measurements obtained at Kew with a rate of decrease in PG of 7.87 V/m per decade or 0.32% per year. This draws one early conclusion that the global signal of PG seems to be decreasing over this time period of 56 years.

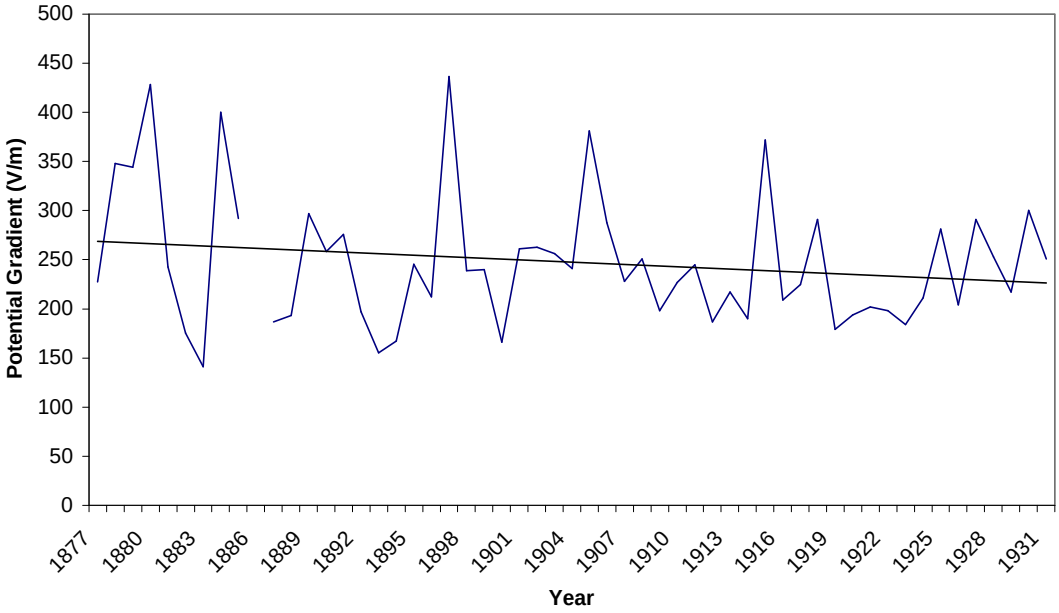

Figure 6.2. Graph showing a time series from 1877-1931 of averaged June global PG measurements made at Kew Observatory. Gap in PG series from 1885-1887 due to value for 1886 being unattainable.

6.2 PG response to temperature

As explained in section 4.3.2 the near surface air temperature record for the tropics and globe was obtained from the Meteorological Office Hadley Centre. In order to correlate the temperature records and PG records, normalisation of the data must be completed. The temperature record is given as the monthly difference from the 1961-1990 mean and so to normalise the PG record, the monthly difference of the 1961-1990 PG must also be obtained. This causes a problem as there are no available PG measurements for the period 1961-1990. The method adopted therefore, is to normalise the PG record as monthly differences from the 1902-1931 (also a 30 year average) values.

6.2.1 Tropical temperatures

Figure 6.3 shows a time series of the normalised PG and tropical near surface air temperatures from 1877-1931. As can be seen from the graph, both the PG and tropical temperatures have some similarities in the trend but during this period, the tropical temperature is increasing (0.006^{o}C/decade) and the PG is decreasing (7.8 V/m/decade). There are some well-defined years where a sharp increase/decrease in temperature also leads to a sharp increase/decrease in PG. In particular sharp increases in temperature and PG occur in 1897, 1907 and 1915 and sharp decreases in the trends occur in 1882, 1884 and 1929.

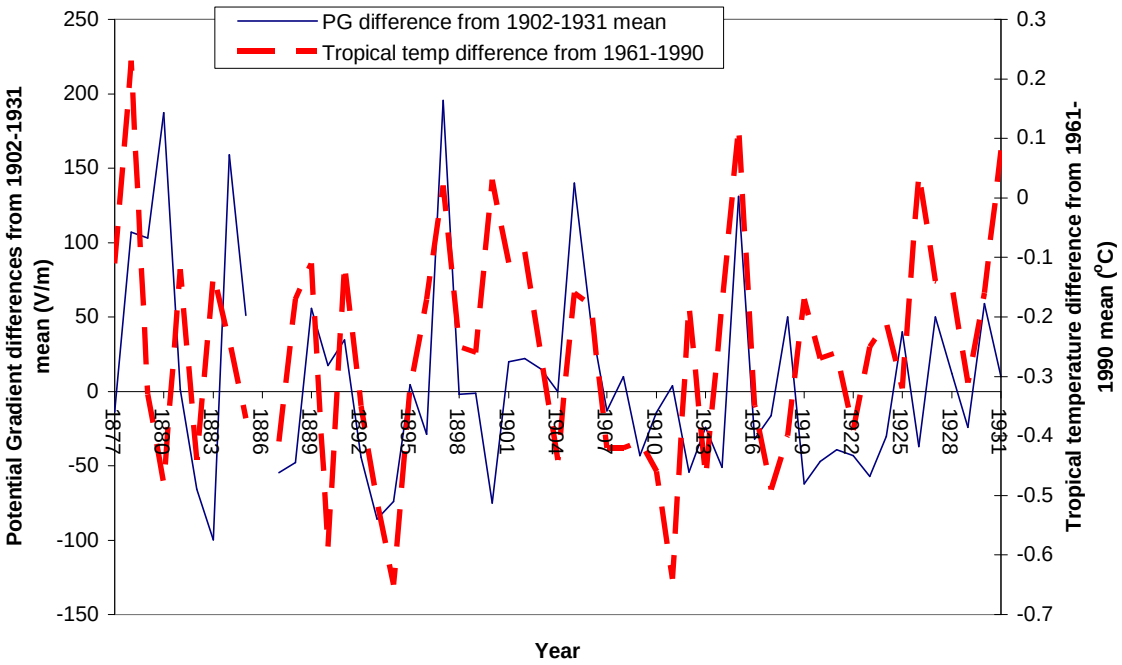

Figure 6.3. Time series of monthly differences from means 1961-1990 and 1902-1931 in tropical temperature (red line) and PG (blue line) respectively from 1877-1931.

By comparing the two time series, there appears to be a small positive correlation between the two series (figure 6.4) with a correlation coefficient of 0.26, which is not a statistically significant correlation.

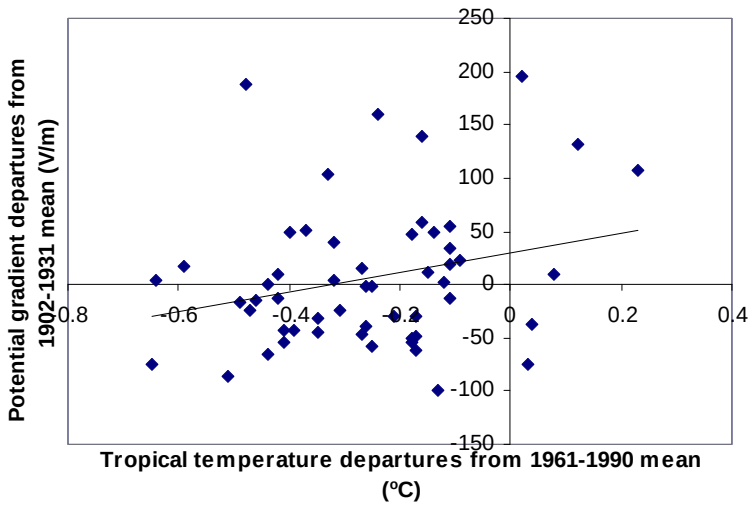

Figure 6.4. Correlation plot of monthly anomalies of tropical temperature and PG from 1877-1931.

When the 1877-1931 tropical temperature and PG are de-trended to remove the low frequency signal, the variations in high frequency signal are very similar to that shown in figure 6.3.

However, when correlating the two variables once the trend has been removed, the correlation becomes significant to 95% (r = 0.27 for 53 values), assuming independent values. Figure 6.5 below shows the correlation plot.

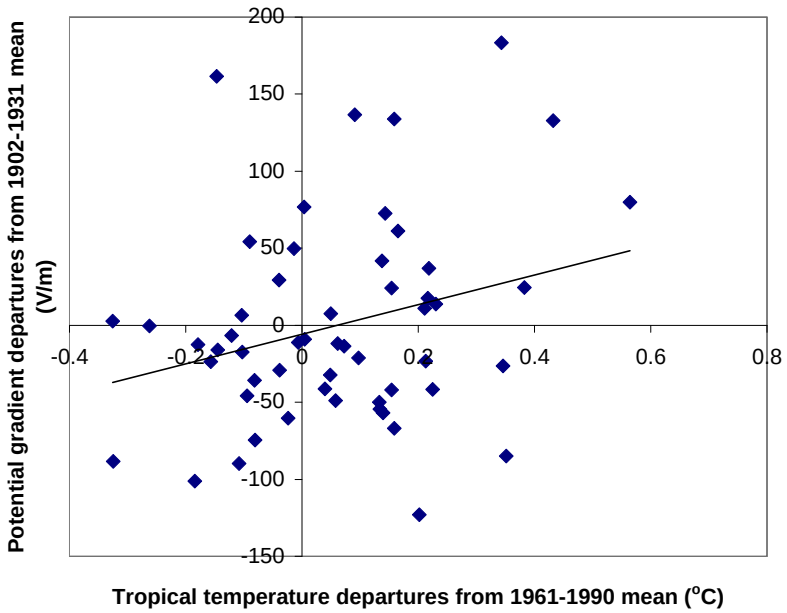

Figure 6.5. Correlation plot of monthly anomalies of de-trended tropical temperature and PG from 1877-1931.

The slope of the linear fit to the data in figure 6.5 provides a sensitivity of how PG changes with tropical temperatures. The data shows a 96 V/m change in PG with a 1°C change in tropical averaged temperature. In terms of sensitivity, this shows a 39% change in PG for every 1°C change in tropical temperatures.

6.2.2 Global temperatures

The global near surface temperature anomalies are also compared with the Kew global signal PG measurements in order to identify any differences from the tropical temperature variations. An independent sensitivity can be established that can be used for more commonly discussed global temperature changes.

Figure 6.6 shows the time series of global near surface air temperature anomalies with the PG anomalies. Both data series have been normalised as discussed in the previous sub-section (6.2.1)

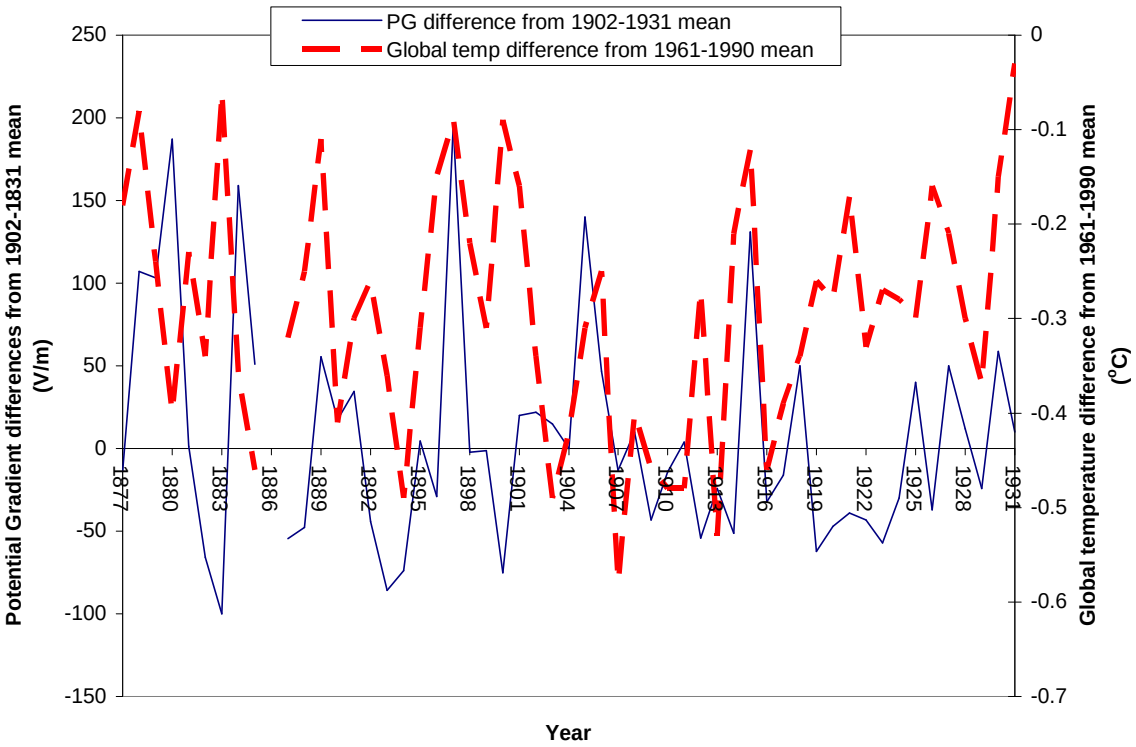

Figure 6.6. Time series of monthly differences from means 1961-1990 and 1902-1931 in tropical temperature (red line) and PG (blue line) respectively from 1877-1931.

This plot shows that during this period, the global near air surface temperatures are cooling by 0.002°C per decade. As in figure 6.3 the PG is decreasing by 7.8 V/m per decade. Despite the difference in annual trend, both data sets once again show some similarities in the shape. Sharp increases in both the global temperature and global PG signal occur in 1897 and 1915 with a sharp decrease in 1930.

Correlation of the two data sets can be seen in figure 6.7 that results in a correlation coefficient of 0.12, which represents a poor positive correlation. As with the tropical temperature and PG, the variations have been de-trended to remove the low frequency signal and have been re-correlated (figure 6.7). The correlation is still poor (r = 0.12 for 53 values) and therefore removing the low frequency signal has no effect on tropical temperature and PG variations.

However, the slope of the linear regression provides a sensitivity of a change in PG of 59 V/m (or 24%) in response to a 1°C change in global temperature.

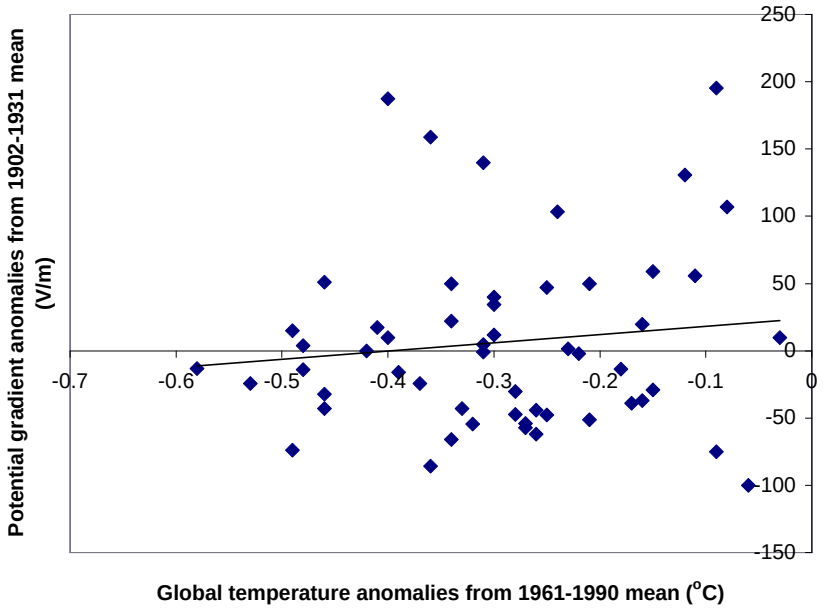

Figure 6.6. Correlation plot of monthly anomalies of global temperature and PG from 1877-1931

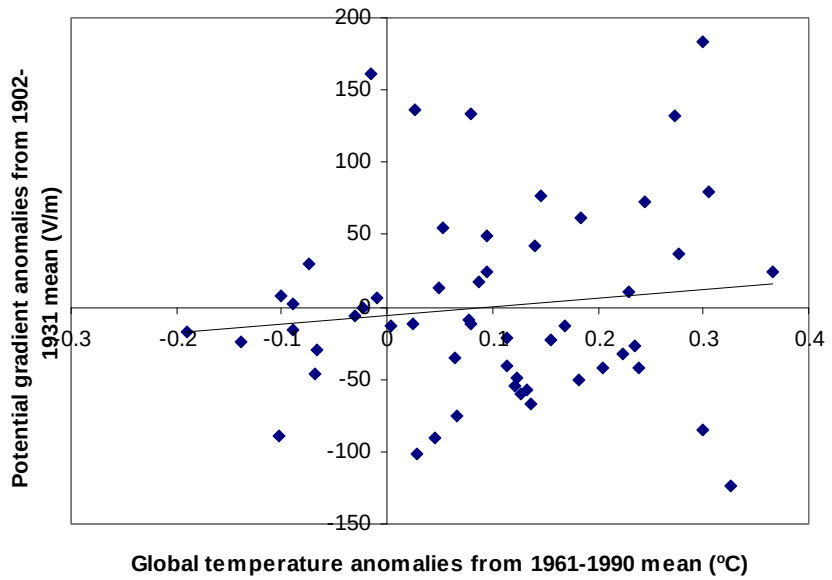

Figure 6.7. Correlation plot of monthly anomalies of de-trended global temperature and PG from 1877-1931.

Chapter 7 – Discussion and conclusions

Global and tropical temperature changes have been suggested as a source of variability in the global atmospheric electric circuit (Williams, 1992; Price, 1993; Markson and Price, 1999). Using an extended time series of PG measurements made at Kew Observatory from 1877-1931, this hypothesis was investigated.

During preliminary analysis to find an absolute calibration, a number of important results were discovered. Local smoke pollution at Kew Observatory produces variability in the local PG, masking a global signal. It was found that the period when local smoke pollution has the lowest influence on PG measurements was in the summer months. Further to this, investigation of the diurnal cycle showed that the PG measured at 1430 UT is least influenced by smoke pollution. It was concluded that this was when a global signal of atmospheric PG is likely. Finding a global signal in the summer months is a reasonable assumption as there is less fossil fuel burning in homes for heating and lighting. This was evident when studying the smoke concentration data at Kew. During the diurnal cycle, there are obvious peaks in the day when a morning and afternoon maximum in pollution occur resulting in an increase in smoke pollution at these times. It is again a reasonable assumption therefore that a global signal may be present at 1430 UT over other times in the day. Despite these results, there are still ion-aerosol interactions in the local atmosphere and using ion-aerosol theory is likely to cause a rise in the local PG. Comparison of extrapolated clean air from Kew was made with PG measurements from Eskdalemuir – known to be a relatively clean air site (Harrison, 2004). Results were promising with Kew 'estimated clean air' PG being 33 V/m higher than Eskdalemuir PG data in the summer months.

Recovery and calibration of 1877-1898 PG data was performed and combined with existing PG data from 1899-1931 (see table 6.2). The absolute calibration method found was a comparison of a direct relationship between relative values of PG and corresponding known values of PG with a measure of the geomagnetic *aa*-index. It was discussed that the *aa*-index is a measure of the average solar magnetic activity at two antipodal stations, which is related to the atmospheric electric circuit due to cosmic ray activity modulating the amount of ionization in the atmosphere and therefore the atmospheric electrical circuit.

A time series of the PG at Kew showed a decrease of 0.32% per year, a result that has not been discussed before. Theory would suggest that a decreasing trend in PG could be explained by a decrease in solar activity. Markson (1981) has suggested that cosmic ray variations modulate the current flowing in the global circuit. A measure of the geomagnetic *aa*-index was used to calibrate 1877-1898 PG data, which theory would suggest is in phase with solar activity indicators such as

sunspot number and inversely related to cosmic ray ionisation (Harrison 2002b). Harrison and Aplin (2002) have shown a decreasing trend in *aa*-index and with evidence from figure 4.4 showing sunspot activity increasing at a rate of 2.4% per year from 1898-1931; these results suggest therefore that the global atmospheric electrical circuit should be decreasing. It is clear therefore that PG measured at Kew in the summer is related to variations in solar activity and *aa*-index.

Comparing the best estimate of a global signal of PG from Kew, with global temperature variations over the period 1877-1931 (figure 6.6) showed a sensitivity of a change in 24% per unit change in global temperature. Using tropical temperature variations, results have shown the PG to change by 39% per unit temperature change. The sensitivities concluded can either mean an increase or decrease in PG with an increase or decrease in temperature. For the period used in this study (1877-1931), the sensitivities stated are decreasing quantities. Results found in this chapter are compared in a summary with other results found by authors listed in table 7.1 below.

Table 7.1. Suggested changes in the global atmospheric electric circuit per 1^{o}C change in global (or tropical) near surface air temperature.

Author	Inferred change in atmospheric electrical circuit per 1^{o}C change in global surface temperature (unless otherwise stated)
Williams, 1992	10% (tropical)
Price, 1993	20%
Price and Rind, 1994	5-6%
Reeve and Toumi, 1998	40%
Markson and Price, 1999	15%

Results range from 5% - 40% with results from this chapter included in this range, providing further evidence of a link between temperature and the global atmospheric electrical circuit. Unlike the majority of authors listed in table 7.1, this study has used a time series stretching 56 years making it significant in a climatological context (>30 year period). Price (1993) uses a dataset from 1983-1990 making it a short 7 year time period that could be providing short term variations in the global circuit. Again, Markson and Price (1999) use 31 balloon soundings of the electrical circuit in 1992 which shows a limited climatological relevance.

The difference in results using tropical and global temperature variations when correlated with PG draws an important conclusion. After removing the low frequency signal of temperature and PG, the near surface global temperatures showed a poor correlation ($r = 0.12$ for 56 values) with PG, whereas the tropical temperature variations showed a significant correlation ($r = 0.27$ for 56 values), assuming independent values. There are a number of explanations for this difference as was highlighted in section 4.3. Firstly, the land/ocean ratio over the tropics remains fairly constant

while outside the tropics, the ratio is much more varied (ref. fig 4.6). Secondly, the lightning distribution over the globe is concentrated in three tropical areas; Africa, South Asia and the border between North and South America. Lastly, the hypothesis presented by Williams (1992) using CAPE theory, whereby higher tropical surface temperatures lead to more vigorous updraft velocity, more upper-cloud ice accumulation and ultimately more lightning. The increased electrical activity in the tropical regions therefore leads to a larger sensitivity with surface temperature changes in this region.

It is important to note that when stating a correlation coefficient and its significance to a 95% confidence interval, assumption was made that values are independent of one another. This assumption contains uncertainties as the PG on a year to year basis may not strictly be independent. It does however give an idea as to how strong the relationships between PG and surface temperatures are, for future guidance in this subject area.

Studying the global atmospheric electric circuit's response to temperature changes is important as it was shown there are a number of climatic feedbacks and increased risks to society. Lighting is a source of atmospheric nitrogen species which reacts with sunlight and oxygen molecules to produce ozone. It was shown that lightning induced NO_x production ranges from 9 to 23%. This results in an increase of tropospheric ozone production by 10% that gives a global radiative forcing of +0.3 W m^{-2}.

Evidence of a link between upper tropospheric water vapour and global lightning activity being correlated was presented. Predictions showed a 10-20% increase in upper tropospheric water vapour for every 1K rise in near surface global temperature, concluding that an increase in upper tropospheric water vapour will amplify surface temperatures from a positive feedback. Evidence of another possible positive feedback was also presented for an increase in CO_2 from the burning of lightning-induced wildfires. Assuming the hypothesis that lightning frequency increases in a warmer climate, a positive feedback is produced.

The risks of an increase in lightning frequency in society were discussed. Current global estimates of deaths caused by lightning are into a thousand with many more thousands injured annually. Other lightning-induced problems to society include property damage, aircraft damage and power failures.

In conclusion, investigation into variations of the global atmospheric electric circuit and it's response to surface temperature changes has raised four major results;

- Recovery, calibration and analysis of NEW PG data series from 1877-1898 at Kew Observatory.

- A clean air PG from a heavily polluted Kew Observatory was well estimated and used as a global signal for the atmospheric electrical circuit.

- There is a POSITIVE relationship between TROPICAL surface temperature variations and global PG estimates.

- There is a weak relationship between GLOBAL surface temperature variations and global PG.

This study has provided up-to-date results on the variability of the global electrical circuit and its response to temperature changes. By doing this there are many other exciting continuation studies that can be investigated and are briefly summarised here;

- Use full extended period of 102 years of Kew PG in investigating the known relationship between both tropical and global near surface with the global atmospheric electrical circuit.

- Fully investigate the local atmospheric electrical circuit at Kew Observatory. Using the PG dataset and ion-aerosol theory it is possible to estimate pollution concentrations from 1877-1989. This will provide further insights into air pollution in London during the early nineteenth century.

- Use of the Climate Diagnostics Centre (CDC) re-analysis package can be used with the PG measurements to find correlations with global near surface air temperature. This could provide spatial analysis of the global atmospheric electrical circuit.

- Other data that may be linked with lightning and thunderstorms, such as rainfall data in Africa can also be used in the CDC re-analysis to find a link between a change in rainfall patterns and thunderstorm activity.

Acknowledgments

I would like to thank Dr. Giles Harrison for all of his very helpful support and guidance throughout the dissertation. I would especially like to thank him for his help in moulding the dissertation into an exciting and (hopefully!) interesting research piece. A massive thank you goes to Emma for putting up with me over the past year – I couldn't have done it without your support.

References

ABBOT, C.G., (1908). Annals of the astrophysical observatory of the Smithsonian Institution, vol II. Smithsonian Institution.

ALDERMAN, E.J., WILLAIMS, E.R., (1996). Seasonal variation of the global electric circuit. J. Geophys Res, **101**, D23, 29679-29688.

D'ALIBARD, T.F., (1752). Letter to Acad. de. Sci.

ANDERSON., R.B., (2001). Does a fifth mechanism exist to explain lightning injuries? IEEE Eng. Med. Biol. Jan/Feb, 105-113.

BAUER, L.A., (1926). Washington Carnegie Institute. Dept. Terr. Mag., Res., **5**, p361.

BERING E.A., FEW, A.A., BENBROOK, J.R., (1999). The global electric circuit. Physics today, **51**, (10), 24-30.

BIGG, E.K., GRAS, J.L., EVANS, C., (1984). Origin of Aitken particles in remote regions of the Southern Hemisphere. J. Atmos. Chem., **1**, 203-214.

CHALMERS, J.A., (1967). Atmospheric Electricity, 2nd Edition. Pergamon Press.

CHAUVEAU, B., (1925). Electricite Atmospherique, 3 vol. Libraire Octave Doin, Paris, France.

CHREE, C., (1896). Observations on atmospheric electricity at the Kew Observatory. Proceedings of the Royal Society of London, **60**, 96-132.

CHREE, C., (1923). London Proc. Physic. Soc., **35**, p129

COBB, W.E., (1968). The atmospheric electric climate at Mauna Loa Observatory, Hawaii. J. Atmos. Sci., **25**, 470-480.

COBB, W.E., PHILLIPS, B.B., (1962). Atmospheric electric results at Mauna Loa Observatory. DOC Tech. Pap. 46, U.S. Dep. of Comm., Weather Bur., Washington, D.C.

EVERETT, J., (1863). Account of observations of atmospheric electricity taken at Windsor, Nova Scotia. Proceedings of the Royal Society of London, **12**, 683-707.

EVERETT, J., (1868). Results of observations of atmospheric electricity at Kew Observatory, and at Kings College, Windsor, Nova Scotia. Philosophical Transactions of the Royal Society, Series A, **158**, 347-361.

FLYGER, H.K., HANSEN, K.., MEGAW, W.J., COX, L.C., (1973). The background level of summer tropospheric aerosol over Greenland and the North Atlantic Ocean. J. Appl. Meteorol., **12**, 161-174.

FRANKLIN, B., (1750). Letter to Royal Society.

HARRISON, R.G., (2002). Twentieth century secular decrease in the atmospheric electric circuit. Geophys. Res. Lett., **29**, (14).

HARRISON, R.G., (2003). Long-term measurements of the global atmospheric electric circuit at Eskdalemuir, Scotland, 1911-1981. Atmospheric Research, **70**, 1-19.

HARRISON, R.G., (2003b). Reply to comment on "Twentieth century secular decrease in the atmospheric potential gradient". Geophys. Res. Lett, **30** (15).

HARRISON, R.G., (2004). Long-term measurements of the global atmospheric electric circuit at Eskdalemuir, Scotland, 1911-1981. Atmospheric Research, **70**, 1-19.

HARRISON, R.G., APLIN, K.L., (2002). Mid-nineteenth century smoke concentrations near London. Atmospheric Environment, **36**, 4037-4043.

HARRISON, R.G., APLIN, K.L., (2003). Nineteenth century Parisian smoke variations inferred from Eiffel Tower atmospheric electrical observations. Atmospheric Environment, **37**, 5319-5324.

HARRISON, R.G., CARSLAW, K.S., (2003). Ion-aerosol-cloud processes in the lower atmosphere. Reviews of Geophysics, **41**(3), 1012.

HOGG, A.R., (1950). Air-earth current observations in various localities. Arch. Meteor., **3**, 40-55.

HANSEN, J., LACIS, A., RIND, D., RUSSEL, G., STONE, P., FUNG, I., REUDY, R., LERNER, J., (1984). Climate sensitivity: Analysis of feedback mechanisms, in Climate Processes and Climate Sensitivity. Geophys. Monogt. Ser., **29**, edited by Hansen , J and Takahashi, T. AGU, Washington, D.C.

HUNTRIESER, H., SCHLAGER, H., FEIGL, C., HOLLER, H., (1998). Transport and production of NO_x in electrified thunderstorms: Survey of previous studies and new observations at mid-latitudes. J. Geophys. Res., 103, 28247-28264.

IPCC, (2001). Climate change 2001: The scientific basis. Summary for policymakers and technical summary of the IPCC WGI Third Assessment Report.

INSTITUTE DE PHYSIQUE DU GLOBE DE PARIS website - http://tango.cetp.ipsl.fr/~isgi/lesdonne.htm (accessed on 27th June 2004).

ISRAEL, H., (1970). Atmospheric Electricity, Vol I. Israel Program for Scientific Translations. Jerusalem, Israel.

ISRAEL, H., (1973). Atmospheric Electricity, Vol II. Israel Program for Scientific Translations. Jerusalem, Israel.

KRIDER, E.P., ROBLE, R.G., (1986). Studies in Geophysics: The Earth's electrical environment. National Academy Press, Washington, D.C.

LEMONNIER, L.G., (1752). Observations sur l'electricite de l'air. Mem. Acad. Sci, **2**, 233.

LIOU, K.N., (1980). An introduction to atmospheric radiation. Academic Press.

MACKERRAS, D., (1985). Automatic short-range measurement of the cloud flash to ground flash ratio in thunderstorms. J. Geophys. Res., **90**, 6195-6201.

MACKERRAS, D., DARVENIZA, M., (1998). Global lightning: Total cloud and ground flash estimates. J. Geophys Res, **103**, (D16), 19791-19809.

MARKSON, R.J., (1985). Aircraft measurements of the atmospheric electrical global circuit during the period 1971-1984. J. Geophys. Res., **90** (D4), 5967-5977.

MARKSON, R.J., LANE-SMITH, D., (1994). Global change monitoring through the temporal variation of ionospheric potential. AMS conference on the global electrical circuit, 273-278, Nashville, Tennessee.

MARKSON, R.J., PRICE, C., (1999). Ionospheric potential as a proxy index for global temperature. Atmos. Res **51**, 309-314.

MARKSON, R.J., RUHNKE, L.H., WILLIAMS, E.R., (1999). Global scale comparison of simultaneous ionospheric potential measurements. Atmos. Res., **51**, 315-321.

MAYAUD, P.N., (1972). The aa indices: a 100 year series characterizing the magnetic activity. J. Geophys. Res., 77, 6870-6874.

METEOROLOGICAL OFFICE HADLEY CENTRE -

http://www.metoffice.com/research/hadleycentre/CR_data/Annual/HadCRUG.gif (accessed on 26t^{h} June 2004)

MILLER, S.L., (1953). A production of amino acids under possible primitive Earth conditions. Science, **117**, 528-529.

MUHLEISON, R.P., (1971). New determination of the air-earth current over the ocean and measurements of ionospheric potentials. Pure Appl. Geophys., **84**, 112-115

NESBITT, S.W., ZHANG, R., ORVILLE, R.E., (2000). Seasonal and global NO_x production by lightning estimated from the Optical Transient Detector (OTD). Tellus B, **52**, 1206-1215.

NOAA Lightning safety website - http://www.lightningsafety.noaa.gov/ (accessed on 16th June 2004)

OTD data website - http://thunder.nsstc.nasa.gov/data/OTDsummaries/ (accessed on 17th June 2004)

PARKSON, W.C., TORRESON, O.W., (1931). The diurnal variation of the potential gradient of atmospheric over the oceans. UGGI Bulletin, **8**, 340-345.

PRICE, C., (1993). Global surface temperatures and the atmospheric electrical circuit. Geophysical Research Letters, **20**, (13), 1363-1366.

PRICE, C., (2000). Evidence for a link between global lightning activity and upper troposphere water vapour. Nature, **406**, 290-293.

PRICE, C., RIND., D., (1994). Possible implications of global climate change on global lightning distributions and frequencies. J. Geophys Res, 99, (D5), 10823-10831.

PRICE, C., PENNER, J., PRATHER, M., (1997). NO_x from lightning. 1. Global distribution based on lightning physics. J. Geophys. Res., **102**, 5929-5941.

RAKOV, V.A. UMAN, M.A., (2003). Lightning: Physics and Effects. Cambridge University Press.

REEVE, N., TOUMI, R., (1998). Lightning activity as an indicator of climate change. Q. J. R. Meteorol. Soc., **125**, 893-903.

RIND, D., CHIOU, E.W., CHU, W., LARSON, J., OLTMANS, S., LERNER, J., MCCORMICK, M.P., MCMASTER, L., (1991). Positive water vapour feedback in climate models confirmed by satellite data. Nature, **349**, 500-502.

SCRASE, F.J., (1934). Observations of atmospheric electricity at Kew Observatory: A survey of the results obtained from 1843 to 1931. Geophysical Memoirs, vol **60**. Meteorological Office, HMSO, London, UK.

SENTMAN, D.D., FRASER, B.J., (1991). Simultaneous observations of Schumann resonances in California and Australia: Evidence for intensity modulations by the local height of the D-region. J. Geophys. Res., **96**, 15793-15984.

SIMPSON, G.C., (1910). Atmospheric electricity in high latitudes. Phil. Trans. A, **205**, 61-97

SINHA, A., TOUMI, R., (1997). Tropospheric ozone, lighting, and climate change. J. Geophys. Res., **102**, (D9), 10667-10672.

SVERDRUP, H.U.M., JOHNSON, W., FLEMING, R.H., (1942). The Oceans: Their physics, chemistry and general biology. Prentice-Hall, Inc.

TOUMI, R., HAIGH, J.D., LAW, K.S., (1996). A tropospheric ozone-lightning-climate feedback. Geophys. Res. Lett., **23**, 1037-1040.

TIE, X., ZHANG, R., BRASSEUR, G., LEI, W., (2002). Global NO_x production by lightning. J. Atmos. Chem., **43**, 61-74.

USDA forest service website - http://www.fs.fed.us/fire/news_info/index.html (accessed on 16th June 2004)

WATSON, R.E., (1929). Measurements of the effective electrical conductivity of the air and the earth's electrical field at and near ground level by means of the Wilson Universal electrometer. Geophys. Mem., London, **45**.

WHIPPLE, G.M., (1881). Observations of atmospheric electricity at the Kew Observatory during 1880. Report of the British Association, p443.

WHIPPLE, F.J.W., (1929). On the association of the diurnal variation of electric potential gradient in fine weather with the distribution of thunderstorms over the globe. Q. J. R. Meteorol. Soc., **55**, 1-17

WILLIAMS, E.R, (1992). The Schumann resonance: A global tropical thermometer. Science, **256**, 1184-1187.

WILLIAMS, E.R., (1994). Global circuit response to seasonal variations in global surface air temperature. Mon Weath Rev, **122**, 1917-1929.

WILSON, C.T.R., (1916). On some determination of the sign and magnitude of electric discharges in lightning flashes. Proc. Camb. Phil. Soc., **13**, 363-382.

WILSON, C.T.R., (1920). Investigations on lightning discharges and on the electric field of thunderstorms. Philosophical Transactions of the Royal Society, Series A, **221**, 73-115.

Appendix 1

Tables below show the relative values taken for each fair-weather days in the June of each year between 1877 and 1898. The average values in red are those copied to table 6.1 (section 6.2.2). Relative values represent a measure of the distance (cm's) away from zero PG.

June 1877

Fair-weather days	0730	1430	Max value	Min value
29th	3	7	13	0
Average for year	3.00	7.00	13.00	0.00

June 1878

Fair-weather days	0730	1430	Max value	Min value
2nd	28	4	36	2
3rd	20	18	36	0
15th	18	8	28	3
22nd	17	6	32	2
Average for year	20.75	9.00	33.00	1.75

June 1879

Fair-weather days	0730	1430	Max value	Min value
5th	26	6	33	1
6th	0	4	14	0
16th	2	2	17	1
17th	6	8	22	2
18th	5	8	22	4
Average for year	5.50	5.60	21.60	1.60

June 1880

Fair-weather days	0730	1430	Max value	Min value
5th	29	20	43	12
11th	25	21	51	15
27th	25	19	41	16
28th	20	24	42	11
Average for year	24.75	20.00	44.25	13.50

June 1881

Fair-weather days	0730	1430	Max value	Min value
10th	13	7	34	1
22nd	10	1	19	1
24th	18	5	45	1
26th	6	12	25	3
28th	15	7	2.7	2
Average for year	12.40	6.40	25.14	1.60

June 1882

Fair-weather days	0730	1430	Max value	Min value
19th	21	15	46	5
23rd	14	22	34	3
Average for year	17.50	18.50	40.00	4.00

June 1883

Fair-weather days	0730	1430	Max value	Min value
20th	8	16	26	0
29th	3	15	36	1
Average for year	5.50	15.50	31.00	0.50

June 1884

Fair-weather days	0730	1430	Max value	Min value
10th	40	31	48	19
11th	40	29	48	11
15th	10	31	62	9
Average for year	30.00	30.33	52.67	13.00

June 1885

Fair-weather days	0730	1430	Max value	Min value
5th	30	28	52	0
14th	45	21	66	1
25th	23	19	66	0
Average for year	32.67	22.67	61.33	0.33

June 1886

NO DATA

June 1887

Fair-weather days	0730	1430	Max value	Min value
4th	7	3	22	1
7th	8	1	17	1
13th	12	6	18	0
19th	10	9	18	0
Average for year	9.25	4.75	18.75	0.50

June 1888

Fair-weather days	0730	1430	Max value	Min value
3rd	10	0	15	0
15th	16	11	24	0
19th	18	9	24	6
Average for year	14.67	6.67	21.00	2.00

June 1889

Fair-weather days	0730	1430	Max value	Min value
10th	28	29	37	3
18th	29	24	34	20
28th	16	16	23	9
Average for year	24.33	23.00	31.33	10.67

June 1890

Fair-weather days	0730	1430	Max value	Min value
1st	26	19	32	16
18th	11	9	22	9
Average for year	18.50	14.00	27.00	12.50

June 1891

Fair-weather days	0730	1430	Max value	Min value
6th	14	13	19	10
18th	20	18	28	15
20th	19	17	28	15
26th	30	27	40	22
27th	34	31	40	28
Average for year	23.40	21.20	31.00	18.00

June 1892

Fair-weather days	0730	1430	Max value	Min value
2nd	11	23	32	7
10th	12	18	31	14
30th	35	16	50	14
Average for year	19.33	19.00	37.67	11.67

June 1893

Fair-weather days	0730	1430	Max value	Min value
3rd	10	6	11	4
Average for year	10.00	6.00	11.00	4.00

June 1894

Fair-weather days	0730	1430	Max value	Min value
16th	9	10	13	1
19th	11	11	20	8
28th	10	8	15	6
29th	11	7	18	4
Average for year	10.25	9.00	16.50	4.75

June 1895

Fair-weather days	0730	1430	Max value	Min value
13th	26	23	30	16
15th	32	27	42	26
25th	21	24	35	16
Average for year	26.33	24.67	35.67	19.33

June 1896

Fair-weather days	0730	1430	Max value	Min value
14th	18	4	25	1
28th	7	9	15	1
Average for year	12.50	6.50	20.00	1.00

June 1897

Fair-weather days	0730	1430	Max value	Min value
2nd	45	11	90	10
6th	10	10	66	1
10th	18	17	55	10
11th	48	14	62	14
14th	20	7	53	1
Average for year	28.20	11.80	65.20	7.20

June 1898

Fair-weather days	0730	1430	Max value	Min value
4th	16	10	45	2
5th	7	7	35	7
7th	13	7	19	5
17th	17	10	24	6
Average for year	13.25	8.50	30.75	5.00